


RESEARCH

Open Access



The down-regulation of XBP1, an unfolded protein response effector, promotes acute kidney injury to chronic kidney disease transition

Jia-Huang Chen¹, Chia-Hsien Wu¹, Jia-Rong Jheng^{1,2}, Chia-Ter Chao^{1,2}, Jenq-Wen Huang², Kuan-Yu Hung², Shing-Hwa Liu¹ and Chih-Kang Chiang^{1,3,4*} 

Abstract

Background: The activation of the unfolded protein response (UPR) is closely linked to the pathogenesis of renal injuries. However, the role of XBP1, a crucial regulator of adaptive UPR, remains unclear during the transition from acute kidney injury (AKI) to chronic kidney disease (CKD).

Methods: We characterized XBP1 expressions in different mouse models of kidney injuries, including unilateral ischemia–reperfusion injury (UIRI), unilateral ureteral obstruction, and adenine-induced CKD, followed by generating proximal tubular XBP1 conditional knockout (XBP1^{CKO}) mice for examining the influences of XBP1. Human proximal tubular epithelial cells (HK-2) were silenced of XBP1 to conduct proteomic analysis and investigate the underlying mechanism.

Results: We showed a tripartite activation of UPR in injured kidneys. XBP1 expressions were attenuated after AKI and inversely correlated with the severity of post-AKI renal fibrosis. XBP1^{CKO} mice exhibited more severe renal fibrosis in the UIRI model than wide-type littermates. Silencing XBP1 induced HK-2 cell cycle arrest in G2M phase, inhibited cell proliferation, and promoted TGF-β1 secretion. Proteomic analysis identified TNF receptor associated protein 1 (Trap1) as the potential downstream target transcriptionally regulated by XBP1s. Trap1 overexpression can alleviate silencing XBP1 induced profibrotic factor expressions and cell cycle arrest.

Conclusion: The loss of XBP1 in kidney injury was profibrotic, and the process was mediated by autocrine and paracrine regulations in combination. The present study identified the XBP1-Trap1 axis as an instrumental mechanism responsible for post-AKI fibrosis, which is a novel regulatory pathway.

Keywords: Unfolded protein response, XBP1, Fibrosis, Acute kidney injury, Chronic kidney disease

Background

Acute kidney injury (AKI) is featured by an abrupt loss of kidney function, associated with high morbidity and mortality, especially in hospitalized patients [1]. Evidence suggests that AKI contributes to an increased risk of long-term cardiovascular events, fractures, infections as well as the progression of chronic kidney disease (CKD) and end-stage renal disease (ESRD) development [2–5].

*Correspondence: ckchiang@ntu.edu.tw

¹ Graduate Institute of Toxicology, College of Medicine, National Taiwan University, No.1 Jen Ai road section 1, Taipei 100, Taiwan
Full list of author information is available at the end of the article



© The Author(s) 2022. **Open Access** This article is licensed under a Creative Commons Attribution 4.0 International License, which permits use, sharing, adaptation, distribution and reproduction in any medium or format, as long as you give appropriate credit to the original author(s) and the source, provide a link to the Creative Commons licence, and indicate if changes were made. The images or other third party material in this article are included in the article's Creative Commons licence, unless indicated otherwise in a credit line to the material. If material is not included in the article's Creative Commons licence and your intended use is not permitted by statutory regulation or exceeds the permitted use, you will need to obtain permission directly from the copyright holder. To view a copy of this licence, visit <http://creativecommons.org/licenses/by/4.0/>. The Creative Commons Public Domain Dedication waiver (<http://creativecommons.org/publicdomain/zero/1.0/>) applies to the data made available in this article, unless otherwise stated in a credit line to the data.

Clinically, ischemia–reperfusion injury (IRI) is the most common etiology of AKI, involving renal tubular injury and death [6, 7]. Aberrant tubular repair may be a critical promoter for the transition from AKI to CKD [4, 8, 9]. Maladaptive repaired proximal tubular cells adopt a partial epithelial-mesenchymal transition (partial EMT) phenotype, which is characterized by cell cycle arrest in the G2/M phase, the activation of transcription factor Snai1, and secretion of profibrotic factors: transforming growth factor β 1 (TGF β 1) and connective tissue growth factor (CTGF) [9–11]. Intriguingly, TGF β 1 stimulates G2/M arrest and the production of profibrotic cytokines in tubular cells, leading to perivascular fibroblasts pericyte-myofibroblast trans-differentiate into myofibroblasts and contributing to renal fibrosis in various animal models of AKI-induced fibrosis [12, 13]. Mechanisms responsible for AKI to CKD transition are complex and involve apoptosis, autophagy, cell cycle arrest, inflammation, ER stress, mitochondria dysfunction, and senescence. Despite this complexity, there is still an unmet medical need in uncovering potential therapeutic targets for patients with AKI to CKD transition.

Endoplasmic reticulum (ER) is responsible for protein synthesis, processing, and transport, and it is essential for maintaining cellular homeostasis. Insults disturbing ER functions lead to ER stress, followed by the induction of unfolded protein response (UPR) which is crucial for maintaining ER proteostasis [14]. Dysregulated ER is associated with disease progression, especially for renal fibrosis, which has been reported in many studies ER stress is involved in AKI to CKD transition [15–18].

During ER stress, three transmembrane stress sensors PKR-like ER kinase (PERK), activating transcription factor 6 (ATF6) and inositol-requiring enzyme 1 α (IRE1 α) are activated to regulate protein synthesis, degradation, and folding capacity. Activation of the PERK-eIF2 α axis inhibits global protein translation while paradoxically inducing the selective translation of ATF4 and the activation of the integrated stress response [19]. ATF6 is proteolytically activated by site-1 and site-2 proteases (S1P and S2P) in Golgi apparatus [20], and the released transcriptionally active N-terminal domain upregulates genes encoding ER chaperones involved in ER-associated protein degradation (ERAD) [21]. IRE1 α activation undergoes conformational changes to promote its dimerization, oligomerization, trans-autophosphorylation, RNase activation and eventually leads to unconventional splicing 26 nucleotides of X-box binding protein 1 (XBP1) mRNA to produce spliced XBP1 (XBP1s). XBP1 mRNA ordinarily translates into an unspliced isoform of XBP1 (XBP1u) and is spliced into the transcription factor XBP1s during ER stress stimulation. Activated XBP1s function as an effector protein response for regulating

UPRs targeting gene by elevating protein folding capacity, ER chaperones expression, ER expansion and ERAD regulation [22, 23]. XBP1s also determines cell fate via relieving ER stress or initiating apoptosis in the presence of irreversible ER stress, whereas XBP1u, encoded from unspliced XBP1 pre-mRNA, regulates the stability, expression and transcriptional activity of XBP1s [24–26].

Although the activation of UPR has been implicated in the pathogenesis of diabetic nephropathy, congenital nephrotic syndrome, and interstitial renal fibrosis [16, 17, 27], the connection between UPR and profibrogenic signaling has not been well explored. Our previous work demonstrated that overwhelming ER stress was significantly activated in the unilateral ureteral obstruction (UUO)-induced renal fibrosis and coincident with attenuation of XBP1 expression, adaptive UPR effector [17]. In order to explore the potential therapeutic role of adaptive UPR in renal fibrosis, we further study the critical molecule XBP1 in the AKI to CKD transition. The decreased tubular XBP1 expression enhances post-AKI fibrosis by inducing DNA damage response and consequent cell cycle G2/M arrest, followed by the activation of profibrotic signaling.

Materials and methods

Mice

XBP1^{fl/fl} mice were kindly provided by Dr. Laurie H. Glimcher (Weill Cornell Medicine, New York, NY, USA) and *Slc5a-CreERT2* mice were purchased from National Laboratory Animal Center-Rodent Model Resource Center (Taipei, Taiwan). XBP1 proximal tubular conditional knockout mice are generated by breeding the *Slc5a-CreERT2* mice with a *XBP1*^{fl/fl} mice. Genotyping was performed on genomic DNA extracted from toes by PCR with specific primers listed in Additional file 1: Table S1. All animal experiments were approved by National Taiwan University College of Medicine and College of Public Health Institutional Animal Care and Use Committee (IACUC No. 20150030, 20170540). Experimental protocols and animal care were provided according to the guideline for the care and use of animals established by National Taiwan University.

Animal models

UUO, unilateral ischemia–reperfusion injury (UIRI), and adenine-induced nephropathy were used in this study. UUO, bilateral ischemia–reperfusion injury (BIRI), and UIRI with contralateral nephrectomy (UIRI + Nx) are commonly used animal models for studies of ischemic AKI and post-AKI fibrosis. Recently, it is reported that UIRI without contralateral nephrectomy (hereafter described as UIRI) induces renal pathology closely resembling those of patients with nephropathy [28]. With

optimized control of animal's body temperature during ischemia, UIRI causes long-term expression of tubular injury markers, fibrosis-related genes, and the deposition of extracellular matrix, suggesting that UIRI can be useful for studying post-AKI fibrosis. C57BL/6 mice aged from 10 to 12 weeks were anesthetized and subjected to 30 min left kidney UIRI. The left kidney of the euthanized animal was clamped for 30 min at 37.5 °C, followed by sera and tissue collection at 1, 3, 5, 11 and 15 days after UIRI (Additional file 2: Fig. S1a). Mice body temperature were monitored by a homeothermic monitor system (Physitemp Instruments Inc., Clifton, NJ, USA) and maintained at 37.5 °C during surgery. For UUO model, the left ureter was obstructed by two-point ligations at the ureteropelvic junction with 4–0 silk sutures through a left flank incision. The sham group underwent the same surgical procedure without clamping renal pedicles or ureter ligation. All animals were sacrificed after 7 days of UUO. For adenine induced CKD, the regular chow diet of LabDiet 5001 (TestDiet) containing 0.25% adenine was purchased from Bio-cando incorporation (Taoyuan, Taiwan). Chronic adenine nephropathy was induced by feeding animals with or without 0.25% adenine diet alternately for 5 weeks (2 weeks adenine diet then 1 week chow diet for rest). Mice receiving regular chow served as the control group. For UIRI with contralateral nephrectomy (UNx) model performed in XBP1 transgenic mice, all mice subjected to 30 min of UIRI then conduct contralateral nephrectomy before 1 day of sacrifice and sacrificed at day 15. Mice serum were collected to detect serum creatinine (Scr) and blood urea nitrogen (BUN) levels using FUJI DRI-CHEM 4000i (Fujifilm, Tokyo, Japan).

Reagents and antibodies

The following antibodies were used: anti-phospho-IRE1 α (NB100-2323) was from Novus Biologicals (Littleton, CO, USA); anti-IRE1 α (#3294) and anti- γ H2AX (#2577) were from Cell Signaling Technology (Danvers, MA, USA); anti-phospho-PERK (SC-32577), anti-PERK (SC-13073), anti-p21 (SC-6246), anti-Chk1 (SC-8408), anti-Cyclin B1 (SC-245), anti-Cyclin D1 (SC-246) and anti-XBP1 (SC-7160) for detecting XBP1s in animal model were from Santa Cruz Biotechnology (Dallas, TX, USA); anti-H2AX (ab124781) and anti-XBP1 (ab37152) for detecting XBP1u in the animal model and in HK-2 cells were from Abcam (Cambridge, UK); anti- α -smooth muscle actin (GTX100034), anti-Trap1 (GTX102017) and anti-vimentin (GTX100619) were from Genetex Inc. (Irvine, CA, USA); anti-GAPDH (G8795) was from Sigma-Aldrich (St. Louis, MO, USA); anti-ATF6 was kindly provided by Dr. Jim-Tong Horng (Chang Gung University, Taiwan) [29]. Anti-mouse IgG (H+L) and

anti-rabbit IgG (H+L) antibodies were purchased from Genetex. The XBP1 siRNA (5'-CCUUGUAGUUGAGAA CCAGGAGUUA-3') and siNTC (medium GC of Stealth negative control duplex) were purchased from Thermo Fisher Scientific (Waltham, MA, USA) and transfected into cells with TransIT-X2 (Mirus Bio, Madison, WI, USA) according to the manufacturer's manual. The Smart Quant Green master mix for the real-time quantitative assay was purchased from Protech (Taipei, Taiwan). Human TGF β 1 Detection enzyme-linked immunosorbent assay (ELISA) kit was purchased from R&D Systems (Minneapolis, MN, USA) and used according to the manufacturer's instructions.

Cell culture

HK-2 and 293 T cells were obtained from Bioresource Collection and Research Center (Hsinchu City, Taiwan) and were cultured in Dulbecco's Modified Eagle Medium (DMEM): F12 (1:1) or DMEM medium (Thermo Fisher Scientific) supplemented with 10% fetal bovine serum (FBS; Thermo Fisher Scientific) at 37 °C in a 5% CO₂-humidified environment.

Plasmid construction and cell transfection

The XBP1s and Trap1 were amplified by PCR from the cDNA prepared from HK-2 cells using the following primers. For XBP1s: 5'-ATCggCTAgCATggATTATA AggATgACgACgATAAAGTggTggTggCAGCCgCg-3', 5'-CgATgCTAgCTTAgACACTAATCAGCTggggAAA-gAgTTC-3'. The product was inserted into the NheI sites of pLKO-AS3w-puro (Academia Sinica, Taipei, Taiwan). For Trap1: 5'-ATTAggTACCATggCgCgCgAgCTgCg-3', 5'-ATgAgAATTCCAgTgTCgCTCCAgggCC-3'. The product was inserted into the KpnI and EcoRI sites of pcDNA3.1(+)/myc-His B (Thermo Fisher Scientific). For the transfection conditions, 40 nM of siRNA and 1 μ g of plasmid for a 35 mm dish was premixed with TransIT-X2 reagent (Mirus Bio) according to the manufacturer's protocol.

Conditioned medium collection and procedure

The conditioned medium was collected from HK-2 cells silenced of XBP1 for 48 h. After collecting the supernatants, the conditional medium was transferred to culture 293 T cells for 48 h.

Histological analysis

For histology assessment, fixed kidneys were paraffin-embedded and sectioned into 4- μ m sections and were stained with Periodic Acid-Schiff (PAS) and Masson's trichrome to estimate renal histological injury and renal fibrosis. For PAS staining, deparaffinized and rehydrated renal sections were stained with 0.5% periodic acid for

5 min and then stained with Schiff reagent for 15 min, followed by counterstaining with hematoxylin solution for 1 min. For Masson's trichrome staining, deparaffinized and rehydrated sections were stained with Bouin's fixative overnight and then stained with Weigert's iron hematoxylin solution and Biebrich scarlet-acid fuchsin solution. After incubating in phosphomolybdic-phosphotungstic acid solution, collagen was determined by staining with aniline blue. The collagen-stained renal sections were quantified by ImageJ software (NIH, <http://rsbweb.nih.gov/ij/>). In brief, the red channel of RGB stack images was selected to set the blue-stained fibrosis area and the whole tissue area separately. The blue-stained area to cross the whole image is represented as fibrosis fraction for the degree of interstitial collagen deposition. Fifteen cortical tubulointerstitial fields that were randomly selected at 200× magnification were assessed in each mouse, and the average for each group was analyzed. The images were acquired using an Olympus BX51 microscope equipped with an Olympus DP72 camera and cellSens Standard 1.14 software (Olympus, Tokyo, Japan).

TUNEL assay

The DeadEnd™ Fluorometric TUNEL System (Promega, Madison, WI, USA) was used for detecting DNA damage in renal tissue. The procedure followed the manual description. Briefly, the paraffin-embedded tissue slide was deparaffinized and rehydrated. After fixing with 4% paraformaldehyde for 15 min, the tissue section was incubated with proteinase K and then incubated with the nucleotide mixture containing fluorescein-12-dUTP and terminal deoxynucleotidyl transferase. 200× magnification fields were randomly captured, and the counts of fluorescent DNA damage cells were counted.

Gene expression analysis

Total RNAs of fresh kidney samples were extracted with TRIzol reagent (Life Technologies, Grand Island, NY, USA) according to the manufacturer's protocol. Total RNA of HK2 cells were extracted using GENzol™ TriRNA Pure Kit (Geneaid, New Taipei City, Taiwan). After DNase treatment, 1 µg of RNA was reverse transcribed with iScript reverse transcription supermix (Bio-Rad, Hercules, CA, USA). The resulting cDNA products were amplified with specific primer pairs to detect mRNA abundance using a StepOnePlus real-time polymerase chain reaction (PCR) system (Thermo Fisher Scientific). The expressions of the target genes were calculated using the relative comparative quantitation method. The sequences of the primer pairs are listed in Additional file 1: Table S1.

Western blotting

Cells were lysed with RIPA lysis buffer (Cell Signaling Technology), and cell debris were removed by centrifugation at 14,000 rpm for 10 min at 4 °C. The protein concentrations were measured by the Coomassie Protein Assay Reagent (Thermo Fisher Scientific). Equal amounts of proteins (15–30 µg) were subjected to sodium dodecyl sulfate polyacrylamide gel electrophoresis (SDS-PAGE) and transferred to the polyvinylidene difluoride membrane (Millipore, Billerica, MA, USA). The membrane was blocked with 5% non-fat milk in Tris-buffered saline-Tween (TBST) (0.2% Tween 20 (vol/vol) for 1 h followed by incubating with specific primary antibodies overnight. After washing with PBST, the membrane was incubated with horseradish peroxidase (HRP)-conjugated secondary antibodies and developed with Immobilon Western HRP Chemiluminescent Substrate (Millipore). The chemiluminescent image was captured with the BioSpectrum 810 Imaging System (UVP, Upland, CA, USA).

Immunofluorescence staining

Fresh renal tissue was dehydrated with 30% sucrose for 24 h at 4 °C, then embedded with OCT gel. The 4-µm-thick tissue sections were further permeabilized and blocked with the mixture of 0.1% saponin (Sigma-Aldrich), 1% gelatin (Sigma-Aldrich), 1% BSA (Sigma-Aldrich) or Mouse on Mouse Blocking Reagent (MKB-2213-1, Vector Laboratories, Burlingame, CA, USA) in the PBS for 1 h at room temperature. The primary antibody XBP1 (ab37152, Abcam), phospho-Histone H3 (ab14955, Abcam), and Ki67 (ab15580, Abcam) were incubated at 4 °C overnight. After three times of wash, the renal sections were incubated with Alexa Fluor 568-labeled anti-rabbit (# A-11011, Invitrogen, Carlsbad, CA) or Alexa Fluor 488-labeled anti-mouse (#4408, Cell Signaling Technology) secondary antibodies at room temperature for 1 h. Nuclei were stained with DAPI. The sections were then washed and mounted with ProLong Gold (#9071, Cell Signaling Technology). The images were captured using Leica Dmi8 fluorescence microscopy (Wetzlar, Germany).

MTS [3-(4,5-dimethylthiazol-2-yl)-5-(3-carboxymethoxyphenyl)-2-(4-sulfophenyl)-2H-tetrazolium] assay

The cell growth and proliferation ability were measured with CellTiter 96® Aqueous One Solution Cell Proliferation kit (Promega). The detailed procedure was described as previous [30]. Briefly, HK-2 cells were plated in a 96-well plate. After washing cells with PBS, a fresh culture medium containing 0.2% MTS was added to each well and incubated at 37 °C for 45 min. The absorbance was measured at 490 nm and 650 nm on the

SpectraMax[®] ABS Plus Microplate plate reader (Molecular devices, San Joes, CA, USA). Data were normalized to controls and represented as the proliferation rate of the controls.

Flow cytometric analysis of cell cycle

After washing twice with ice-cold PBS, cells were collected and fixed using 70% ethanol at 4 °C for at least 30 min. Then the cells were washed twice with ice-cold PBS and stained with 50 µg/ml propidium iodide (P4170, Sigma-Aldrich) in the presence of 30 µg RNase A (Thermo Fisher Scientific) at room temperature for 30 min prior to analysis using flow cytometry (BD LSRII, BD bioscience, San Jose, CA, USA) with excitation laser 561 nm and bandpass filter 670/30. Data was output as FACS files and analyzed by FlowJo software (BD bioscience).

Protein identification by LC–MS/MS analysis

Proteomic analysis technical was performed by BIOTOOLS Co., Ltd (New Taipei City, Taiwan). For sample preparation, in-sol digestion was applied. Each sample were first diluted in 100 mM triethylammonium bicarbonate (TEABC), and then reduced with 5 mM tris-(2- carboxyethyl)-phosphine (Sigma-Aldrich), followed by cysteine-blocking with 55 mM iodoacetamide (Sigma-Aldrich). After samples were digested with sequencing-grade modified porcine trypsin (Promega), the peptides were then labeled with dimethyl reagent, pooled, and desalted by homemade C18-microcolumn. Digested peptides were detected through LC–MS/MS analysis (Agilent Technologies, Santa Clara, CA, USA) with reverse column (Zorbax 300SB-C18, 0.3 × 5 mm, Agilent Technologies). The LC apparatus coupled with a 2D linear ion trap mass spectrometer (Orbitrap Classic, Thermo Fisher Scientific) and operated using Xcalibur 2.0.7 software (Thermo Fisher Scientific). For protein identification, the SwissProt database (released on Mar 16, 2016, extracted for Homo sapiens, 20,199 sequences) was searched using the Mascot search engine (Matrix Science, London, UK; version 2.5).

Luciferase reporter assay

Each well of 24-well plate contained 4×10^4 cells transfected with 0.4 µg of Trap1 promoter containing pGL3 luciferase reporter vectors (pGL3-basic) and 0.04 µg of thymidine kinase promoter-Renilla luciferase reporter plasmid (pRL-TK) as an internal control. Trap1 promoter region (– 1315 ~ + 54) is amplified by PCR using primers with built-in restriction sites (Additional file 1: Table S1). The PCR products are digested with NheI and HindIII, and ligated to a NheI and HindIII digested pGL3-basic plasmid. Cells are lysed and assayed for firefly and

Renilla luciferase activity using the dual-luciferase kit (BIOTOOLS). The results are normalized to the Renilla luciferase activity of the internal control.

Chromatin immunoprecipitation (ChIP) assay

Chromatin immunoprecipitation assay was performed using SimpleChIP[®] Enzymatic Chromatin IP Kit (#9003, Cell Signaling Technology). Briefly, approximately 4×10^6 cells were fixed with 1% formaldehyde for 10 min at room temperature then digested with Micrococcal Nuclease and sonicated after 2 sets of 6-s pulses using a VirTis Virsonic 100 Ultrasonic Sonicator at 50% amplitude with a 1/8-inch probe. The DNA–protein complex was immunoprecipitated using anti-XBP1 or anti-IgG antibody overnight at 4 °C. After eluting and purifying, XBP1s binding sequence was evaluated by PCR amplification using Trap1 primer sets as listed in Additional file 1: Table S1.

Statistics

Results are presented as the mean ± standard error of the mean (SEM). Statistical significance of differences was determined by the Student's two-tailed *t*-test or one-way ANOVA with Duncan post-test. A P-value of < 0.05 was interpreted as significant. All experiments were repeated at least three times to ensure reproducibility.

Results

Renal unilateral ischemia–reperfusion injury (UIRI) leads to post-injury fibrosis in mice

First, we confirmed the pathological findings of post-AKI injury in our UIRI model. Periodic acid–Schiff (PAS) staining found the accumulation of debris in the tubular lumen beginning at day 1 post-UIRI (Additional file 2: Fig. S1b). In addition, the expressions of AKI marker, kidney injury molecule-1 (Kim-1), increased with a peak at day 1 post-UIRI and gradually decreased over time (Additional file 2: Fig. S1c). The fibrotic fraction visualized by Masson's trichrome staining showed a 30% increase compared to sham group at day 15 post-UIRI (Additional file 2: Fig. S1d-e). Consistently, the expression of α-SMA increased prominently throughout the course of the experiments (Additional file 2: Fig. S1f-g). In summary, these results demonstrate that UIRI causes prominent renal damage and the development of fibrosis.

Activation and modulation of UPR in UIRI model

Next, we monitored the activation status of UPR in the kidneys of the UIRI model. The results showed that the expressions of phospho-PERK and cleaved ATF6 (cATF6) were upregulated in UIRI kidneys at day 1 post-UIRI, and the peak timing of each molecule was around day 5 and day 3 post-UIRI, respectively

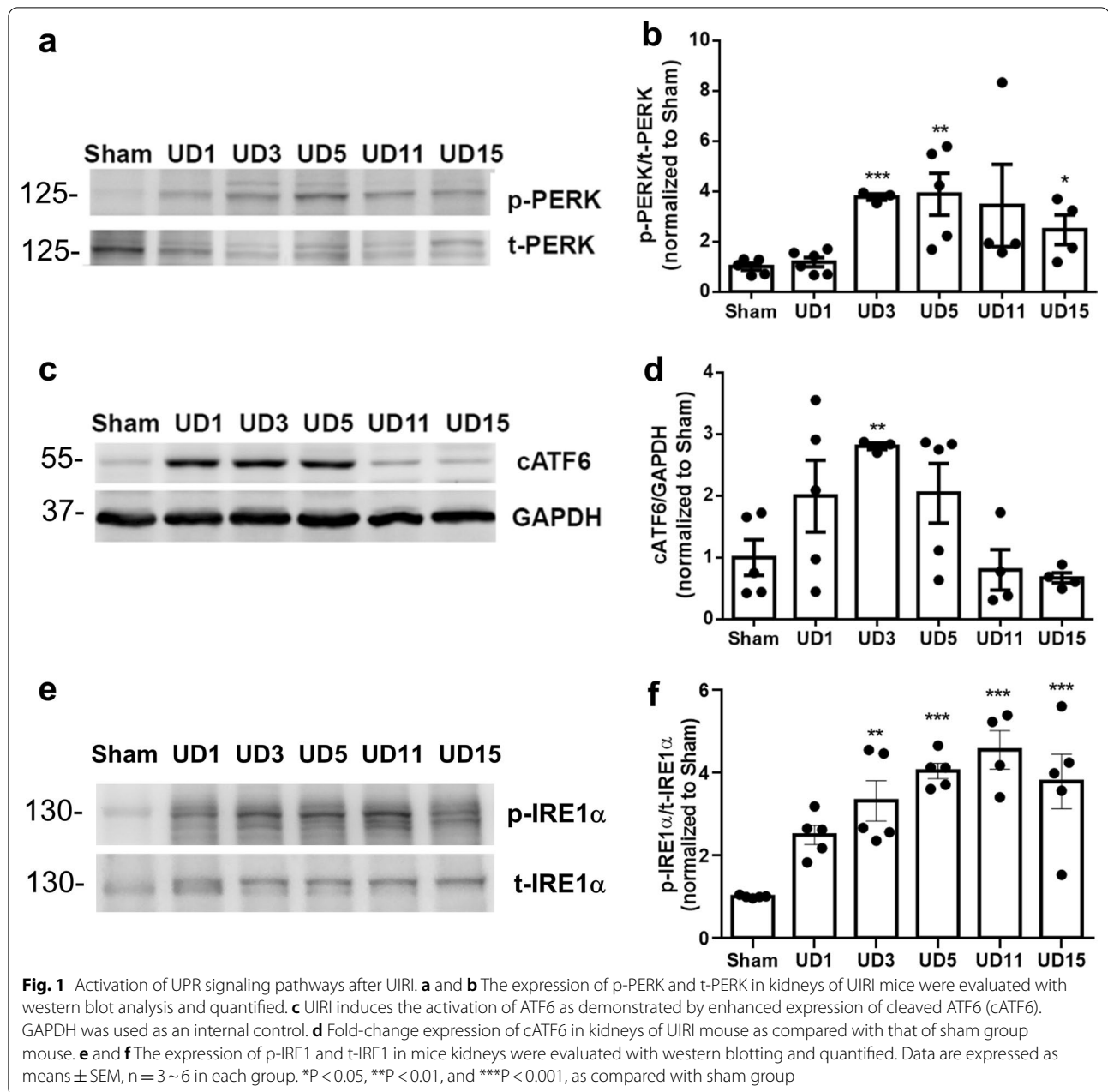
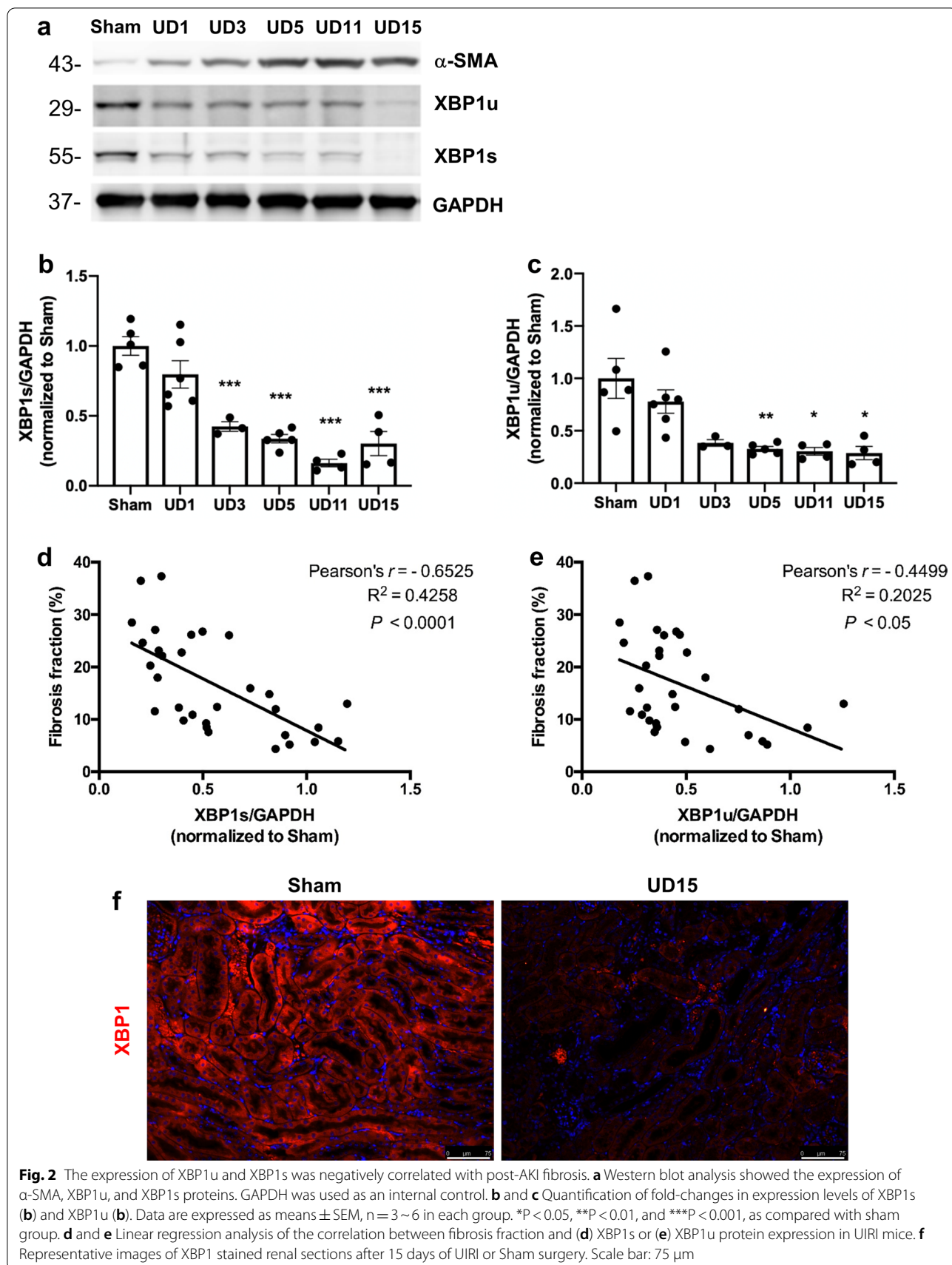


(Fig. 1a–d). Similarly, the expression levels of phospho-IRE1 α were upregulated in UIRI kidneys at day 1 post-UIRI (Fig. 1e). The expression of phospho-IRE1 α in UIRI kidneys slightly decreased at day 15 post-UIRI, but remained substantially higher than sham controls (Fig. 1e). These findings suggest that the activation and modulation of UPR is an early response to UIRI and might influence the development of post-AKI fibrosis.

The role of decreased XBP1u and XBP1s with post-AKI fibrosis

According to our previous finding, overwhelming of ER stress results in IRE1 α phosphorylation and ER-associated degradation leads to selective XBP1u and XBP1s downregulation, which were associated with renal fibrosis progression in UUO model [17]. Hence, we further monitored the contribution of IRE1 α to post-AKI



fibrosis by examining the downstream splicing of XBP1. Both XBP1u and XBP1s protein expression levels were progressively declined following UIRI (Fig. 2a–c), especially in the dilated renal tubular section as shown in the immunofluorescence staining (Fig. 2f); XBP1s (Pearson's $r = -0.6525$, $P < 0.001$; Fig. 2d) and XBP1u protein expression (Pearson's $r = -0.4499$, $P < 0.05$; Fig. 2e) exhibited a significantly negative correlated with the degree of fibrosis. To comprehensively evaluate the expressions of different XBP1 isoforms in various kidney injury models, we measured α -SMA, XBP1u, and XBP1s expression in UUO and the adenine-induced CKD models. Upon model establishment, mice in UUO and adenine models had increased expression of α -SMA and decreased expression of XBP1s and XBP1u (Additional file 2: Fig. S2). Therefore, we propose that XBP1 downregulation can be a common pathway in post-AKI fibrosis.

XBP1 knockout in renal proximal tubules leads to more severe kidney IRI

To specifically investigate the functional role of XBP1 in post-AKI fibrosis, we generated proximal tubular XBP1 conditional knockout (*XBP1^{ckO}*, *Slc5a^{CreERT2}*; *XBP1^{fl/fl}*) mice using the cre/loxP system (Additional file 2: Fig. S3a). After 5 consecutive days of tamoxifen administration (75 mg/kg), the knockout efficacy was evaluated by IP injection of 500 ng/g ER stress inducer-Tunicamycin (TM, 500 ng/g) for 12 h to induce XBP1s expression. And results were performed by western blot analysis and IF staining (Additional file 2: Fig. S3b, c). As Fig. S3b–c western blot analysis and immunofluorescence staining revealed that XBP1s expression was increased in XBP1^{fl/fl} treated with TM group and slightly decreased in XBP1^{ckO} treated vehicle group due to only proximal parts of tubular epithelial cells being knockout. While XBP1^{ckO} mice block TM-induced XBP1s expression. To specifically evaluated XBP1 deletion in the proximal tubular segment, we isolated the renal cortex and medulla fraction of XBP1 transgenic mice to detect XBP1 mRNA expression. The result showed that XBP1s mRNA expression decreased by approximately 65% in the cortex and 35% in the medulla as compared to XBP1^{fl/fl} cortex fraction (Additional file 2: Fig. S3d, e).

To determine whether loss of XBP1 affected post injured renal fibrosis, XBP1^{fl/fl} and XBP1^{ckO} mice subjected to tamoxifen induction then underwent UIRI surgery and were sacrificed 15 days later (Fig. 3a). Masson's trichrome staining of the injured kidney showed that the depletion of tubular XBP1 promoted post-UIRI fibrosis (Fig. 3b and c), and XBP1^{ckO} mice had more significant collagen deposition as evidenced by increased *Colla* mRNA expression (Fig. 3d). Fibrotic markers, including

α -SMA and vimentin, also significantly increased in XBP1^{ckO} mice subjected to UIRI compared to XBP1^{fl/fl} UD15 group (Fig. 3e–g). These data suggested that XBP1 deletion in proximal tubular exacerbated fibrosis development after IRI.

XBP1 specific deletion in proximal tubular aggravates maladaptive repair process

Since progressive fibrosis is associated with the severity of the tubular injury, inflammatory response, and DNA damage response (DDR) [31, 32], the mRNA expression levels of *Kim-1* (kidney injury molecule-1), *Tnf- α* , and *Adgre1* (F4/80) were significantly increased in XBP1^{ckO} UD15 group compared to XBP1^{fl/fl} UD15 group but no difference in *Il-6* mRNA expression (Fig. 4a–d). To specifically investigate renal function impairment in UIRI model, we performed a contralateral nephrectomy in XBP1^{ckO} mice subjected to UIRI before one day of sacrifice (UNx, Additional file 2: Fig. S4a) due to the compensatory effect of the contralateral kidney, UIRI does not affect BUN and Scr levels, as previously described [30]. In comparison to XBP1^{fl/fl} UNx group, XBP1^{ckO} mice exposed to UNx demonstrated significantly higher BUN and Scr levels (Additional file 2: Fig. S4b and S4c). Furthermore, higher levels of the DNA damage marker γ -H2AX were found in XBP1^{ckO} mice with UIRI (Fig. 3h), and we performed TUNEL assay co-staining with XBP1 to examine the relationship between loss of XBP1 and DNA damage. As the results demonstrated that TUNEL positive areas were dissociated from XBP1 stained sections, and the injured tubular in XBP1^{ckO} UD15 group had more DNA fragmentation stained than the XBP1^{fl/fl} UD15 group (Fig. 4e). Collectively, these findings confirm that XBP1^{ckO} mice were more vulnerable to IRI and impaired the subsequent repair processes.

Loss of XBP1 leads to cell cycle G2/M arrest

Recent studies place emphasis on the contribution of injured proximal tubule cells arrest in the G2/M phase to the progression from AKI to CKD, possibly through producing profibrogenic growth factors [10]. We identified similarly the phenomenon of cell cycle G2/M arrest in our UIRI model, evidenced by an elevated protein expression of Chk1, p21, and Ki67⁺pHH3⁺ tubular epithelial cells after UIRI (Additional file 2: Fig. S5a–e). Moreover, Ki67⁺pHH3⁺ areas were obviously increased in XBP1^{ckO} compared to XBP1^{fl/fl} both in sham and UIRI groups (Additional file 2: Fig. S5f–g), suggesting XBP1 deletion in tubular cells prolongs cell cycle arrest in G2M phase and contributes to fibrosis progression.

Next, we further investigated whether XBP1 downregulation was functionally connected with cell cycle regulation. Human renal tubular epithelial cells HK2

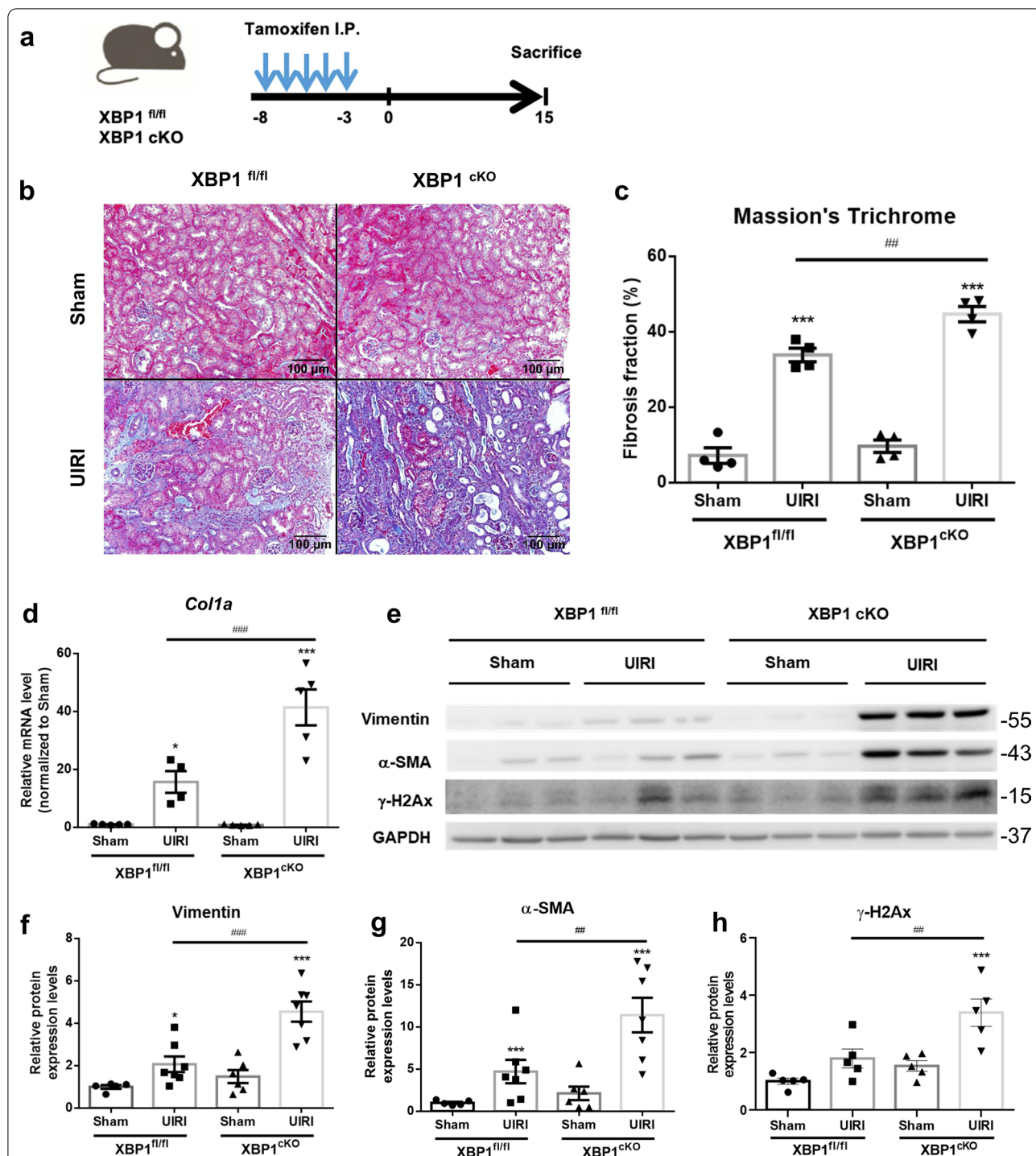
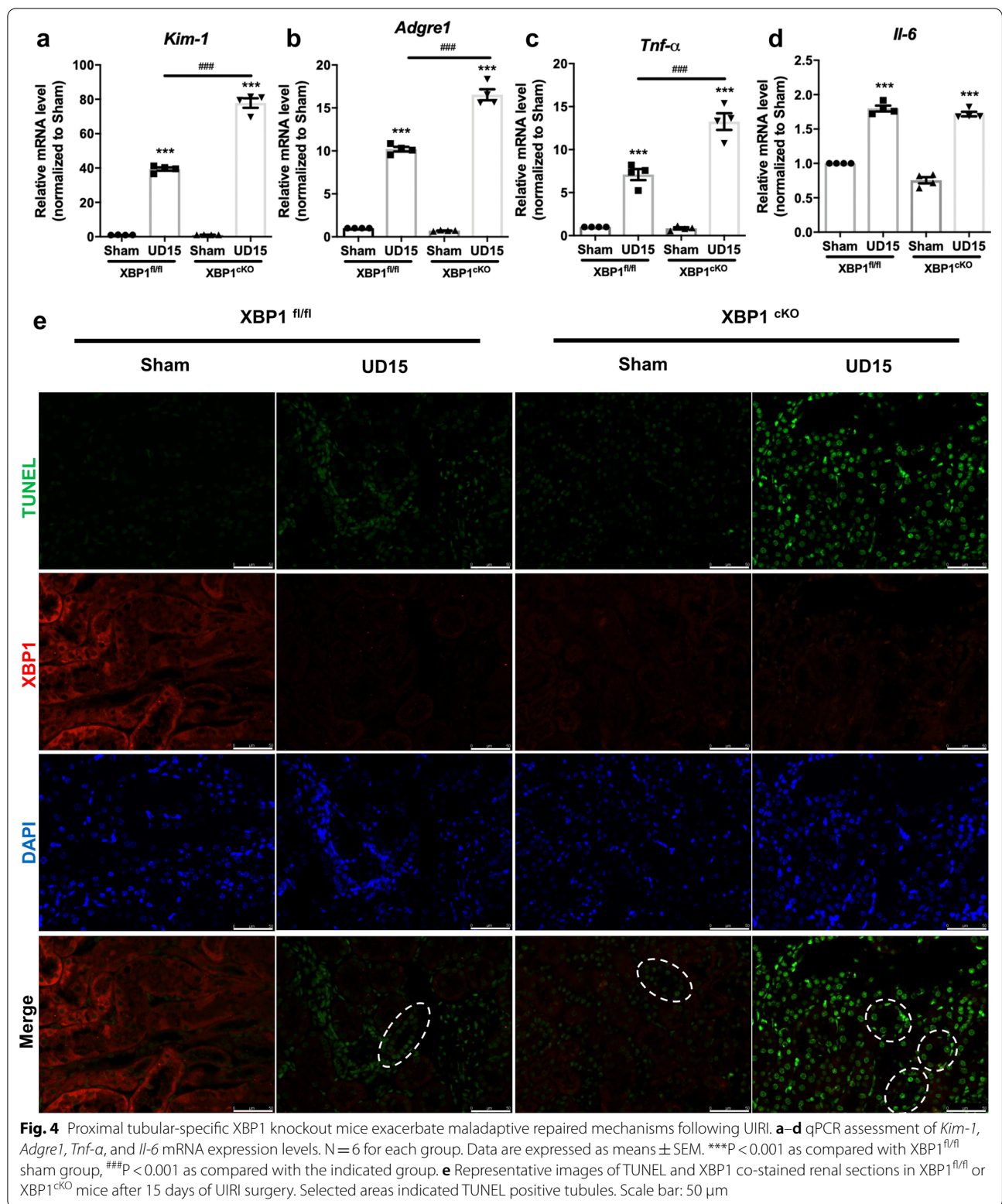


Fig. 3 Specific proximal tubular knockout of XBP1 enhanced renal fibrosis in UIRI mice. **a** Diagram illustrates the timeline of the experiment. All the experimental mice were intraperitoneal injection of tamoxifen, then subjected to UIRI for 30 min. **b** Masson's trichrome staining shows the increased fibrosis fraction in XBP1^{cKO} mice kidney section after UIRI. N = 3–4 for each group. Scale bar indicates 100 μ m in 200 \times . **c** Quantitative scores of interstitial fibrosis were assessed. **d** qPCR assessment of the relative expression level of *Col1a* mRNA. **e–h** The expression of α -SMA and vimentin were examined with western blot analysis and quantified. N = 5–8 for each group. Data are expressed as means \pm SEM. *P < 0.05, *** < 0.001 as compared with XBP1^{fl/fl} sham group, #P < 0.05, ##P < 0.01, ###P < 0.001 as compared with the indicated group



were transfected with either scrambled siRNA (siNTC) or siRNA duplexes against XBP1 (siXBP1), and the silence efficiency was validated by semi-quantitative PCR (Fig. 5a and b). An apparent cell growth inhibition in XBP1-deficient cells compared to scrambled controls was demonstrated by the MTS assay (Fig. 5c). We then assessed the cell cycle status in XBP1-deficient cells using

flow cytometry and found that the percentage of cells in G2/M phase increased in XBP1-silenced cells compared to that in scrambled siRNA-transfected cells (Fig. 5d and e). XBP1-silenced cells exhibited higher cyclin B1/cyclin D1 ratios than scramble controls (Fig. 5f and g). As G2M phase arrest is typical of DDR, we then investigated the potential role of XBP1 in DDR. γ H2AX, a marker of

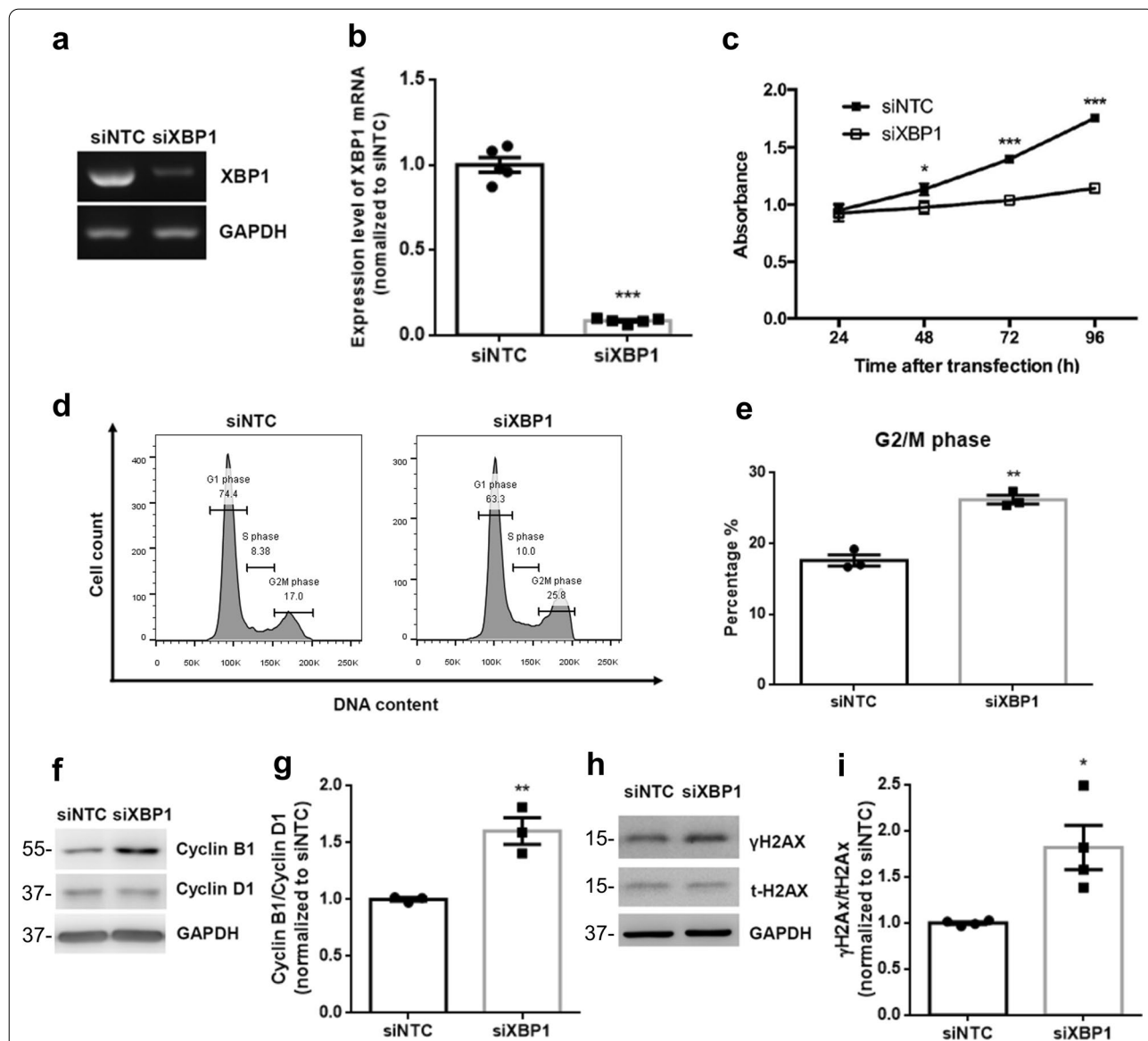


Fig. 5 Knockdown of XBP1 induces cell cycle G2/M arrest in HK2 renal tubule epithelial cells. **a** and **b** The knockdown efficiency of XBP1 was determined by reverse transcription-PCR and quantified. siNTC: negative control siRNA. **c** Loss of XBP1 results in growth inhibition. MTS assay was conducted every 24 h for up to 4 days to examine the effect of XBP1 deficiency on the growth rate of cells based on the absorbance. **d** Loss of XBP1 results in modulating the cell cycle. Cells were transfected with siNTC or siXBP1. After 24 h, cells were harvested and subjected to flow cytometric analysis to determine the cell cycle distribution. **e** The amounts of cells in the G2/M phase of the cell cycle in HK2 cells following transfection of indicated siRNA were quantified. **f** Western blot analysis showed the expression of cyclin B1 and cyclin D1 proteins. GAPDH was used as an internal control. **g** The ratio of cyclin B1 to cyclin D1 in HK2 cells following transfection of indicated siRNA. **h** Western blot analysis showed the expression of γ H2AX and t-H2AX proteins. **i** The ratio of γ H2AX to t-H2AX in HK2 cells following transfection of indicated siRNA. Data are expressed as means \pm SEM of three independent experiments. * $P < 0.05$, ** $P < 0.01$, and *** $P < 0.001$, as compared with siNTC group

DNA damage, significantly increased in XBP1 knock-down cells (Fig. 5h and i). Collectively, these results provide evidence that XBP1 is essential for proper cell cycle progression.

The profibrotic paracrine effect of XBP1 silenced HK2 cells

Maladaptive repair mediated partial-EMT contributes to G2M arrested tubular cells, increasing profibrotic cytokine production, supporting the role of tubular epithelial cells in renal fibrosis initiation and progression [9–11]. Therefore, we examined related genes expression and found *SNAI1*, *CTGF*, and *COL4A1* mRNA expression significantly upregulated in XBP1-deficient cells compared to scramble controls (Fig. 6a). In addition, the amount of secreted active TGFβ1 determined by ELISA, the master regulator of fibrosis, also increased in the culture media from XBP1-deficient cells (Fig. 6b). 293 T human embryonic kidney cells with related undifferentiated phenotypes were used to evaluate the stimulating effect of TGFβ1 released from XBP1 silenced HK-2 conditioned medium (CM). After exposure to siXBP1 CM, 293 T cells exhibited higher expression of fibrotic-associated genes, including TGFβ1, CTGF, COL4A1, and COL1A1, than those of siNTC CM treated cells (Fig. 6c). These results simulate a paracrine effect of XBP1-deficient tubular epitheliums on adjacent renal cells. Furthermore, cumulating studies support the profibrotic effects of TGFβ1 in human kidney diseases. Thus, we investigated the effect of XBP1 deficiency on TGFβ1-mediated profibrotic signaling. HK2 cells were transfected with either siNTC or siXBP1 for 48 h, followed by treatment with vehicle or 5 ng/mL of TGFβ1 for 24 h. These findings reveal that TGFβ1-treated XBP1-deficient cells display an increased G2/M population compared with TGFβ1-treated controls (Fig. 6d, e). Taken together, the presented data show that XBP1 deletion enhanced TGFβ1 secretion in tubular cells, resulting in a vicious cycle that stimulates surrounding cells prolonged cell cycle arrest and profibrotic factors production.

Trap1, a cell cycle-regulated protein, is identified as down-regulated in XBP1 deficiency model

We found XBP1 is essential for HK-2 cells as silencing XBP1 causes cell maladaptive repaired phenotype. Furthermore, XBP-1 is a critical signaling molecule that participated in adaptive UPR; loss of XBP-1 would disrupt downstream effector proteins, making it difficult to maintain the biological processes. Accordingly, we performed proteomic analysis to examine differentially expressed proteins in HK-2 cells silenced of XBP1 compared to scramble control. Among 378 candidate proteins, 26 were up-regulated and 13 were down-regulated (Fig. 7a and Additional file 3). To determine the functional

regulator affected by the loss of XBP1, we searched for all of the significantly changed proteins involved in cell cycle control or fibrosis progression. TNF receptor-associated protein1 (Trap1), a member of the heat shock protein 90 family that participates in cell-cycle regulation [33, 34] and protects against renal tubulointerstitial fibrosis in UUO model [35], was found to be the most reduced protein in our proteomic analysis data. We further validated Trap1 protein expression correspondingly decreased in HK-2 cells silenced with XBP-1 (Fig. 7b and c). Besides, Trap1 protein expression was also evaluated in the low XBP1 expression mice kidney samples, which have been validated in Fig. 2 and Additional file 2: Fig. S2. Findings from UIRI, UUO, and adenine models showed that Trap1 protein decreased in all experimental groups, paralleling the loss of XBP-1 protein (Fig. 7d–i). In addition, XBP1^{ckO} mice also showed relatively lower Trap1 expression both in sham group and UIRI group compared to XBP1^{fl/fl} (Fig. 7j and k). These results support a highly regulatory possibility between XBP1 and Trap1.

Spliced XBP1 transcriptionally regulates Trap1 expression

According to our findings (Figs. 2 and 7), Trap1 expression correlated with those of XBP1. We subsequently explored whether Trap1 was regulated by XBP1 through manipulating XBP1s expression. Trap1 mRNA was upregulated in HK-2 cells transfected with the XBP1s plasmid (Fig. 8a, b). To more specifically investigate XBP1s promoter binding activity, Trap1 promoter sequence was cloned into pGL3-basic plasmid (Fig. 8c). We showed that HK-2 cells transfected with pGL3-Trap1 promoter, pRenilla luciferase, and pAs3w-XBP1s demonstrated a substantial increase in luciferase activity. Moreover, the binding site of XBP1s on Trap1 promoter was confirmed by the ChIP-qPCR assay. Only the Trap1 promoter primer set (Region 3, – 296 ~ – 451) can amplify the signaling from XBP1s antibody pull-down chromatin when HK-2 cells were transfected with XBP1s plasmid (Fig. 8d–f). These results suggest that XBP1s transcriptionally regulates Trap1 expression.

Trap1 overexpression rescues silenced XBP1 induced G2M arrest

As Trap1 has been reported to regulate cell cycle and protect mitochondrial integrity [33], we are curious about whether restoring Trap1 expression would relieve cell cycle arrest. Trap1 overexpression did not affect cell cycle G2M arrest markers, histone H3 phosphorylation and cyclinB1/D1 ratio expressions. However, Trap1 overexpression in XBP-1 silenced group significantly decreased histone H3 phosphorylation and cyclinB1/D1 protein expression compared to siXBP-1 group (Fig. 9a–d). Consistent with western blot results, Trap1

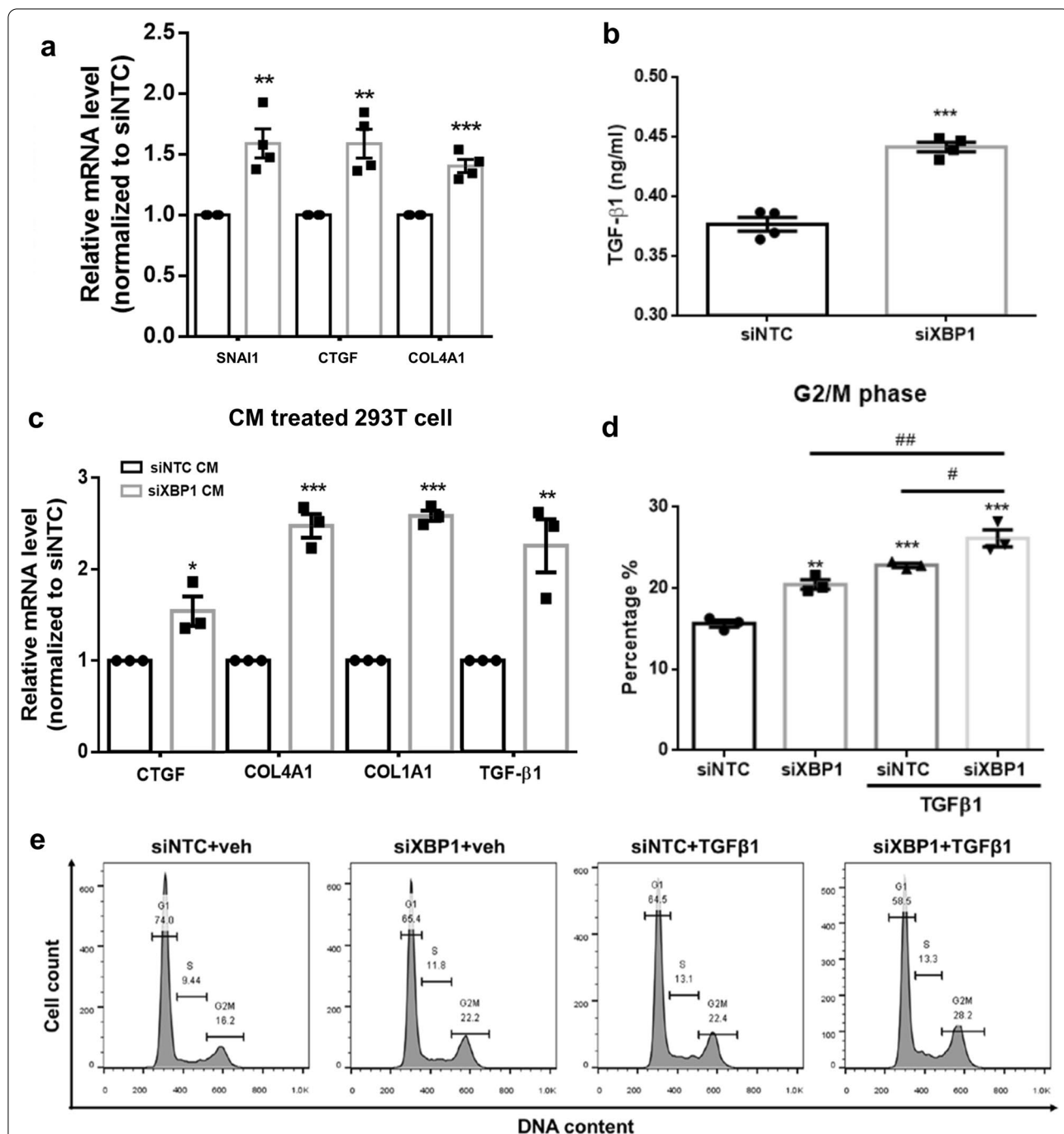


Fig. 6 XBP1-deficient HK2 cells possess profibrotic properties. **a** XBP1 deficiency enhances the mRNA expression of *SNAI1*, *CTGF* and *COL4A1* in HK2 cells. **b** Compared to cells transfected with siNTC, XBP1-deficient HK2 cells secrete elevated levels of active TGF-β1 as assessed by ELISA. **c** Conditioned medium from XBP1-deficient HK2 induces mRNA expression of *CTGF*, *COL4A1*, *COL1A1*, and *TGFβ1* in 293 T cells. **d** Loss of XBP1 sensitizes HK2 cells to TGFβ1-induced cell cycle G2/M arrest. HK2 cells were transfected with indicated siRNA, and 48 h later cells were treated with vehicle (veh) or TGFβ1 (5 ng/mL) for 24 h. Cells were then harvested and subjected to flow cytometric analysis to determine the cell cycle distribution. **e** The amounts of cells in the G2/M phase of the cell cycle were quantified. Data are expressed as means ± SEM of three independent experiments. *P < 0.05, **P < 0.01, and ***P < 0.001, as compared with siNTC group. ##P < 0.01 compared between indicated groups

overexpression attenuated silenced XBP1-induced cell cycle arrest in G2M phase (Fig. 9g and h). Furthermore, profibrotic factor production was also relieved in Trap1 restoration group, evidenced by CTGF protein expression levels in XBP1 deficient and Trap1 overexpression group compared to the XBP1 silenced group (Fig. 9e and f). These results indicate that Trap1 is a regulator capable of preventing the prolongation of cell cycle G2M arrest and reducing profibrotic factor production in XBP1 deficient HK-2 cells.

Discussion

AKI is an important contributor to CKD and ESRD [36]. Patients with AKI are at an increased risk of progressive CKD during hospitalization between 2011 and 2012, according to the United States Renal Data System (USRDS) [4]. Since proximal tubular epithelia exhibit high oxygen demand and contain low antioxidants [37], they are often thought to be the main targets of AKI. During the transition from AKI to CKD, injured tubular epithelial cells play an important role. Partial-EMT, cell-cycle arrest, and imbalanced proteostasis are important factors in post-injury fibrosis [38]. EMT damages renal parenchyma by retarding tubular cell cycle progression, resulting in renal function decline [11]. The production of profibrogenic factors by injured tubular epithelial cells stimulate fibroblast proliferation and collagen synthesis. Furthermore, the association between partial-EMT mediated tubular epithelial cells cell-cycle arrest and renal fibrosis has also been reported [9]. The pathophysiologic role of proteostatic imbalance in injured kidney is supported by in vivo findings of kidney fibrosis amelioration by chemical chaperones or ER stress preconditioning [16, 18, 39]. While these factors exaggerate fibrosis, it is unknown how they interact.

The present study showed that AKI promoted post-injury renal fibrosis in a mouse UIRI model, based on findings of increased expressions of EMT marker, α -SMA, and fibrosis severity on Masson trichrome staining. These results are in accordance with previous findings using both unilateral and bilateral IRI models [40, 41]. In addition, we found that UPR initiators PERK, IRE1 α , and ATF6 were activated following AKI, while the expression of XBP1 gradually lowered throughout

experiments and inversely correlated with the degree of renal fibrosis. We further demonstrated that losing XBP1 caused G2/M cell cycle arrest and inhibited proliferation of proximal tubule epithelial cells. Our findings uncover the role of ER stress master regulator XBP1, which connect cell cycle regulation to the development of renal fibrosis (Fig. 10).

Modulating the expression of XBP1s or XBP1u and its protective role has been reported previously. An ATF6-dependent maladaptive ER response induced by impaired XBP1s nuclear translocation was observed in diabetic nephropathy [42]. In comparison with the control group, nuclear expressions of XBP1s are lower in both murine models of diabetic nephropathy and diabetic patients. Furthermore, the IRE1 α -XBP1 pathway is activated in co-chaperone Sec63-deficient tubule epithelial cells. Double knockout of Sec63 and Xbp1 enhances the severity of polycystic kidney disease in mice and re-expression of XBP1s is able to rescue the inactivation of Sec63 with XBP1 or IRE1 α induced interstitial inflammation and fibrosis [43, 44]. Fan and Xiao et al. showed that the expressions of XBP1s decreased in the kidneys of patients with AKI. Although there was no statistical difference in the amount of XBP1s between stage III AKI patients with and without progression to CKD, a trend toward lower XBP1s expressions in patients with progressive AKI could be observed [15]. Collectively, these findings support the notion that loss of XBP1 potentially contributes to the progression of renal diseases.

As the previous study identified that the hypomorphic variants of XBP1 are the susceptibility factors to spontaneous inflammatory bowel disease [45]; and progressive CKD development is associated with intensive renal inflammation cytokines: *Il-6*, *Tnf- α* , *Adgre1*, and kidney injury molecule *Kim-1* expression. Therefore, we detected the mRNA expression in renal tissue and found that only *Il-6* mRNA expression levels did not significantly upregulate in XBP1^{ckO} UIRI group compared to XBP1^{fl/fl} UIRI group, which could be explained that XBP1s can activate *Il-6* mRNA transcription in cancer cell [46, 47].

Conversely, sustained activation of XBP1s could lead to unfavored responses. Overexpression of XBP1s, for example, has been shown to enhance apoptosis and atherosclerosis progression in human umbilical vein

(See figure on next page.)

Fig. 7 Cell cycle-regulated protein Trap1 is downregulated in the loss of XBP1 models. **a** Protein expression levels in XBP1 deficient HK-2 were presented by MS-based proteomics analysis. The present data shows siXBP1 over siNTC protein expression normalized ratio. **b** and **c** The protein expression of Trap1 in XBP1 silenced HK-2 cell was examined by western blot and quantified. GAPDH was used as an internal control. Data are expressed as means \pm SEM of three independent experiments. * $P < 0.05$. **d** and **e** The protein expression of Trap1 in mice kidneys of UIRI was evaluated with western blotting and quantified. **f** and **g** The protein expression of Trap1 in mice kidneys of UUO was evaluated with western blotting and quantified. **h** and **i** The protein expression of Trap1 in mice kidneys of adenine diet was evaluated with western blotting and quantified. **j** and **k** The protein expression of Trap1 in XBP1^{ckO} mice kidneys was evaluated with western blotting and quantified. Data are expressed as means \pm SEM of at least three independent measurements. * $P < 0.05$, and *** $P < 0.001$, as compared with sham group

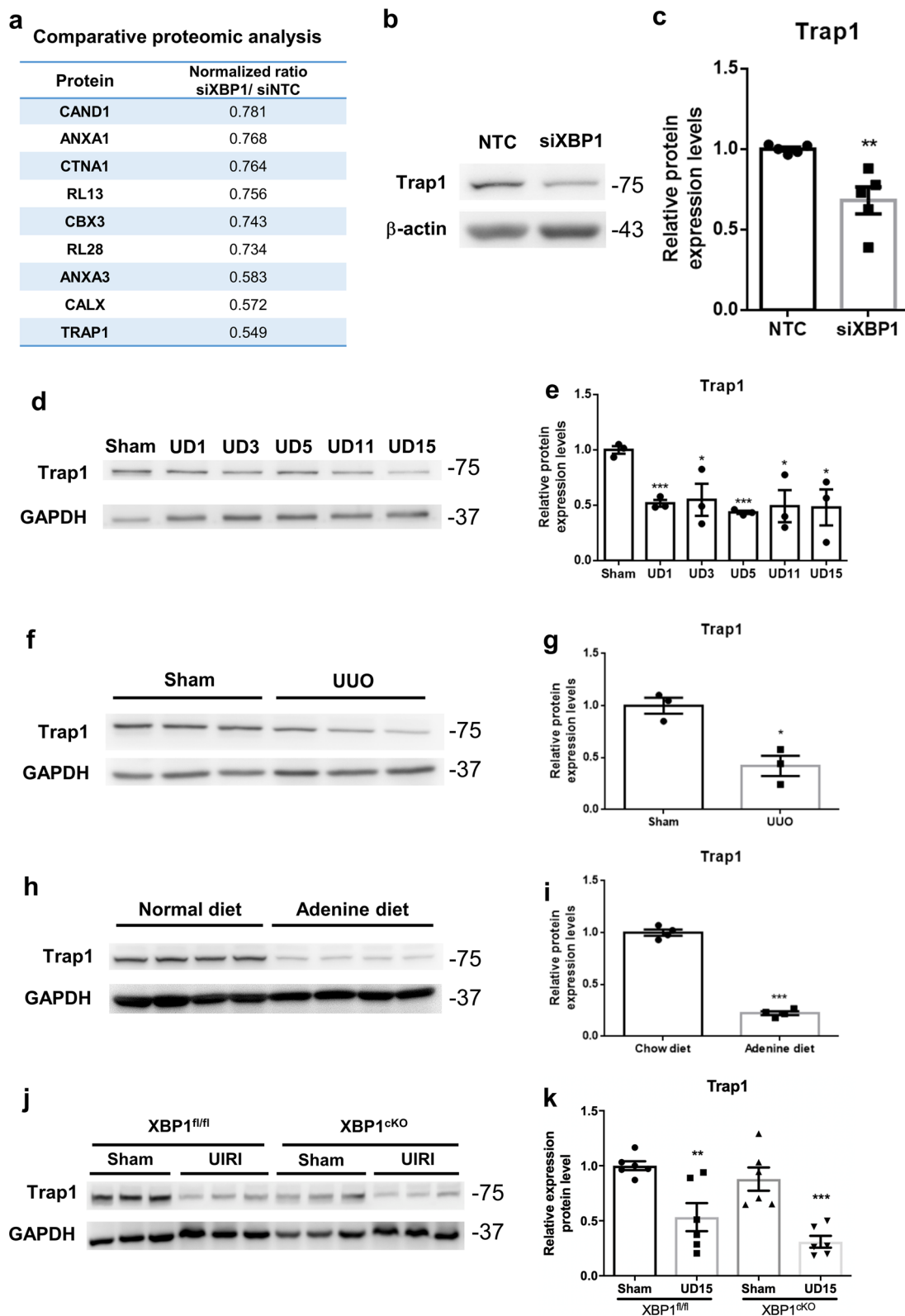


Fig. 7 (See legend on previous page.)

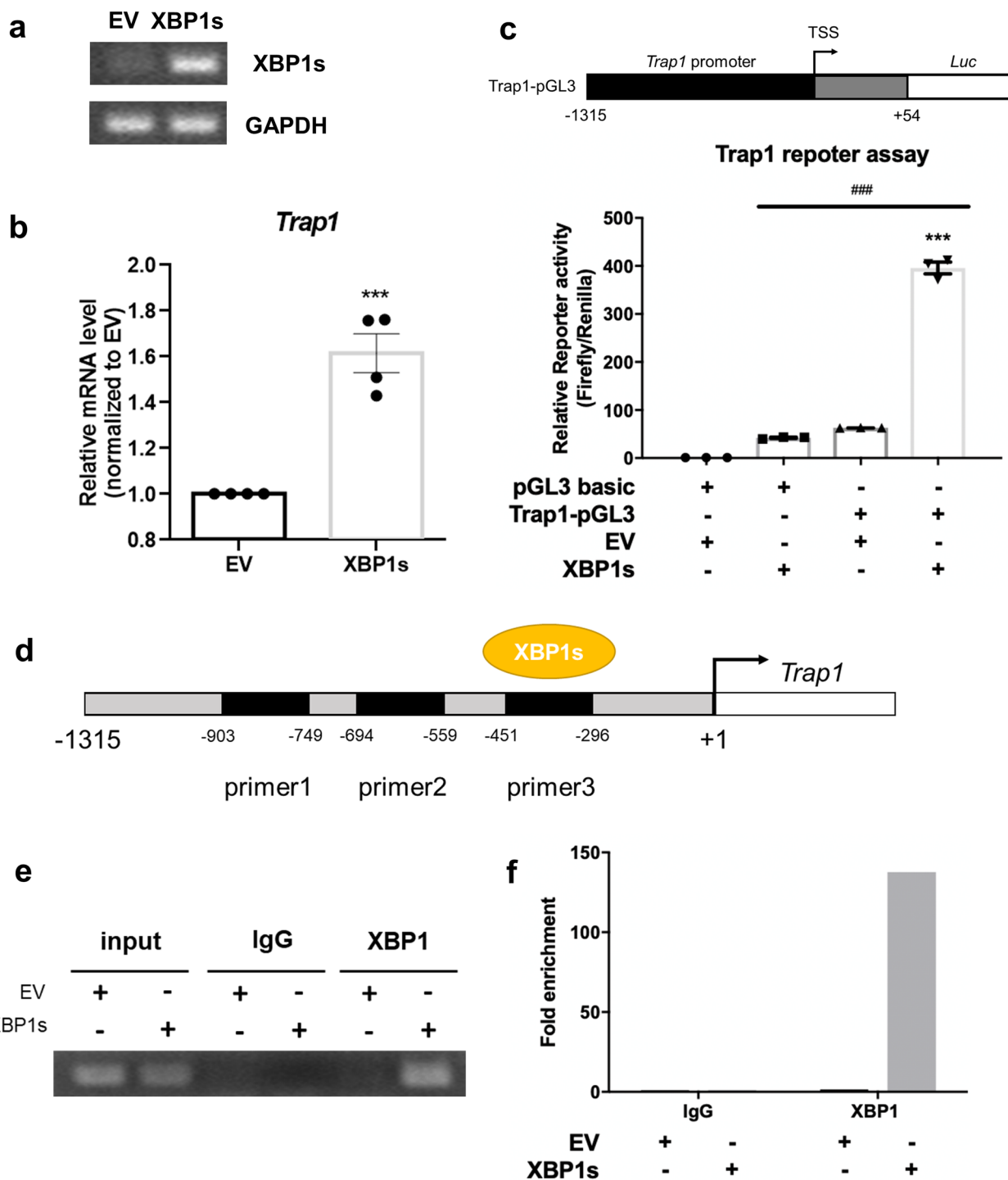
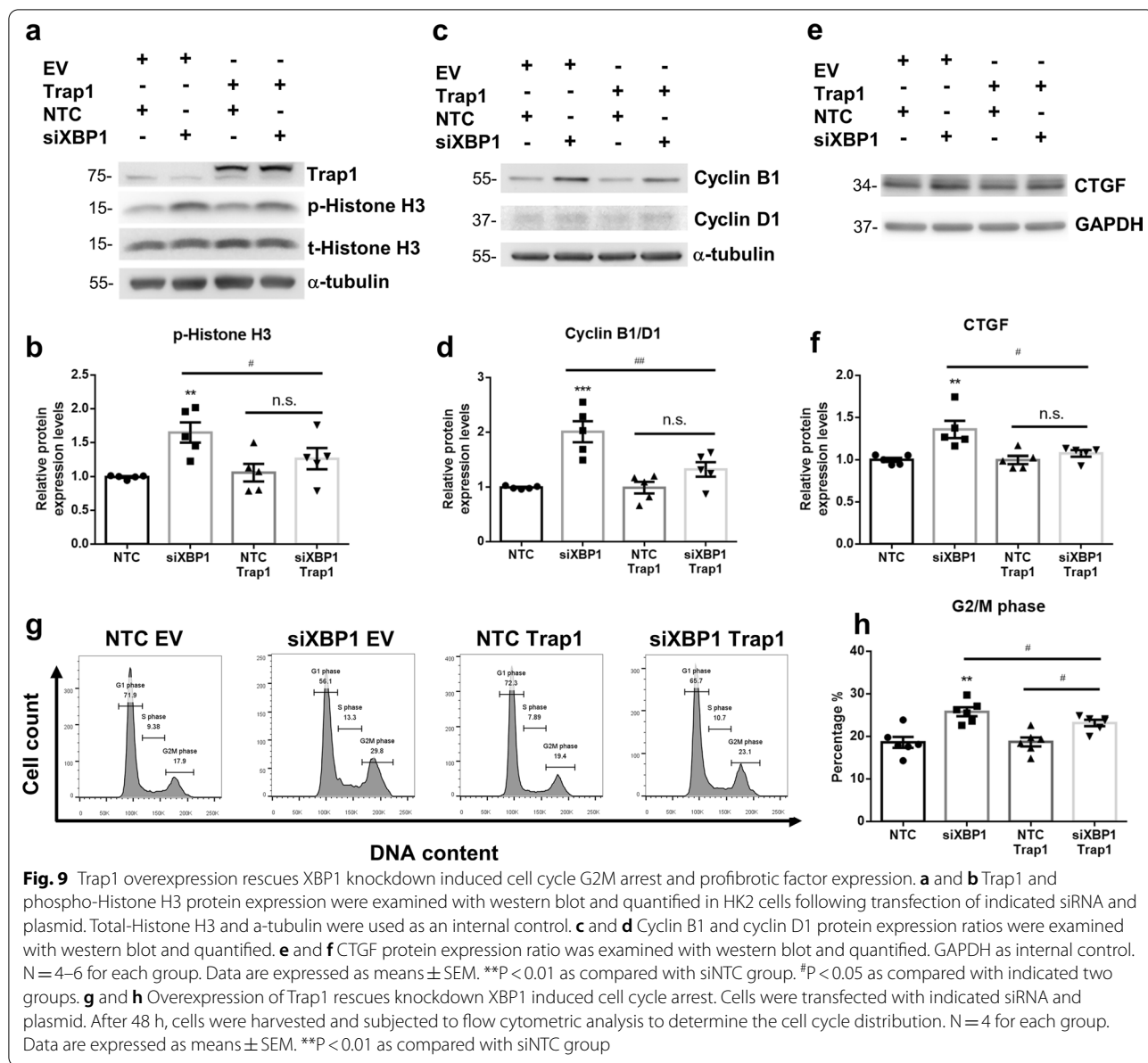


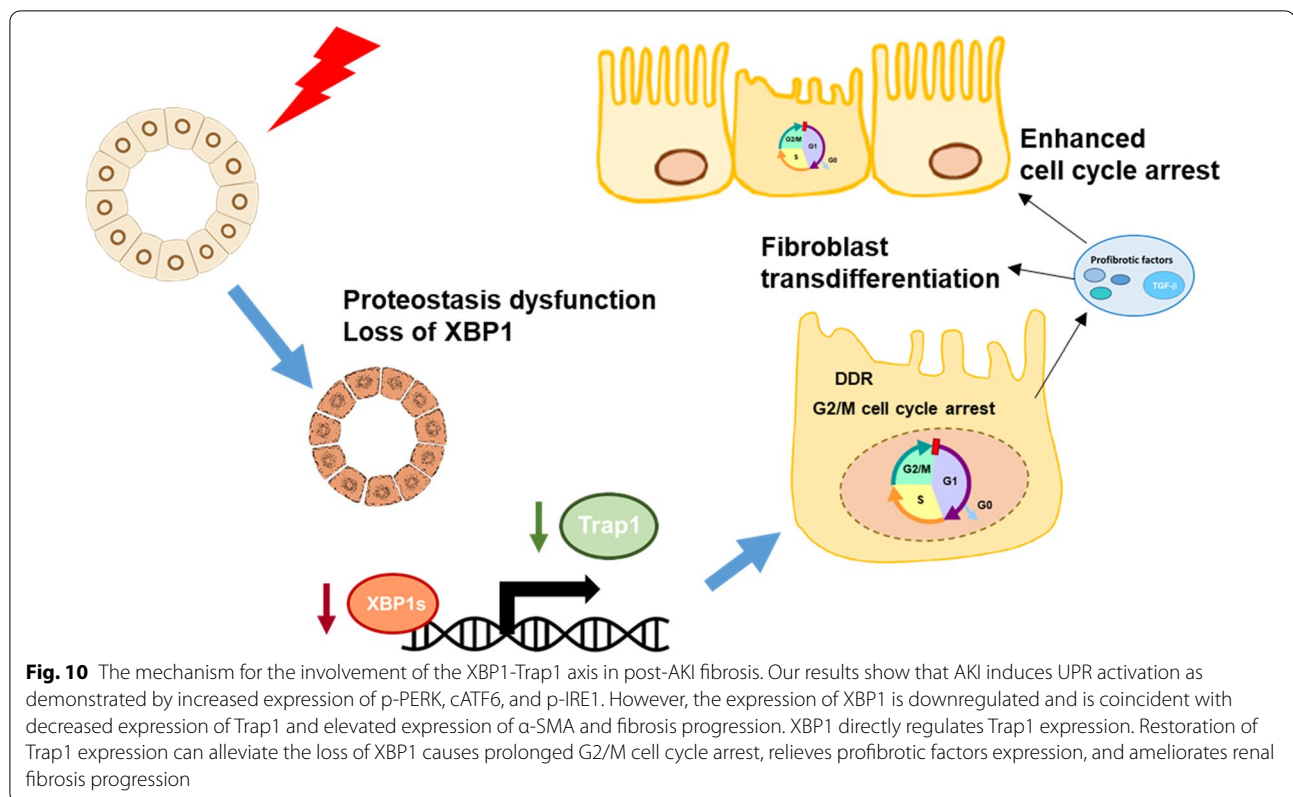
Fig. 8 Spliced XBP1 participated in *Trap1* expression at transcriptional regulation. **a** XBP1s mRNA expression levels were determined by semi-quantitative PCR. HK-2 cells were transfected with 1 μ g of pLAS3W-XBP1s. **b** *Trap1* mRNA expression was evaluated by qPCR in HK-2 cells overexpressed with XBP1s. N = 4 for each group. Data are expressed as means \pm SEM. ***P < 0.0001 as compared with empty vector (EV). **c** *Trap1* promoter binding ability of XBP1 was examined by luciferase reporter assay. Upper panel: schematic diagrams of *Trap1* promoter-luciferase reporter. Lower panel: relative luciferase activity in HK-2 cells transfected with a *Trap1* promoter-luciferase reporter plasmid or empty vector (pGL3 basic), along with EV or XBP1s plasmid. Renilla luciferase activity was used as an internal control and for normalization of transfection efficiency. N = 3 for each group. Data are expressed as means \pm SEM. **d-f** ChIP-PCR assay was performed to analyze the binding of XBP1s to *Trap1* promoter in 293 T cells. **d** Three sets of primer pairs covered the - 296 ~ - 451, - 559 ~ 694, - 749 ~ 903 regions, and qPCR showed that XBP1s bound to - 296 ~ - 451 region (**e** and **f**)



endothelial cells (HUVECs) [48]. Moreover, Moe et al. demonstrated that XBP1s is implicated in Lipopolysaccharide (LPS) induced AKI and inflammation; and manipulating XBP1s overexpress in tubular epithelium can potentiate prolonged LPS exposure induced inflammatory cytokines and kidney injury molecules expression. Although previous studies have shown XBP1s protect against inflammatory disorders like IBD and polycystic kidney disease, Moe’s work highlights the unique role of XBP1s in tubular epitheliums during LPS-induced sepsis.

Given the inconsistent effect of genetic manipulation of XBP1 in disease therapy, the current study applied a

high throughput screening approach to identify non-toxic molecules that selectively activate the IRE1 α -XBP1s arm of the UPR without globally activating other signaling pathways related to ER stress [49]. IXA4, the most selective IRE1 α -XBP1 activator, can promote the degradation of Alzheimer’s disease-associated amyloid precursor protein (APP) mutants, prevent APP-associated mitochondrial dysfunction, and remodel obesity-induced metabolic dysfunction [50]. Based on these encouraging publications and our present findings, the therapeutic effect of IXA4 on AKI to CKD transition is under our investigation and selective activation of IRE1 α -XBP1s signaling in IRI would be clarified in further research.



IRE1 α signaling activates XBP1s expression, while our finding showed that IRE1 α phosphorylation without corresponding XBP1 upregulation but inhibition in the UIRI model. Our previous research showed that overwhelming ER stress induction in UUO with IRE1 α -phosphorylation and ER-associated degradation results in the suppression of XBP1u and XBP1s protein expression, implying the adaptive UPR is disrupted [17]. Similarly, Dufey et al. demonstrated that genotoxic stress arouses IRE1 α activation independent of canonical XBP1 splicing, leading to regulated IRE1 α -dependent decay of mRNA (RIDD) mediated DDR and cell cycle arrest [51]. miRNA also participated in XBP1 regulation. Duan et al. showed that XBP1 is the direct target for miR-214 in the animal model of cardiac hypertrophy and heart failure [52, 53]. Additionally, another study presented by Denby et al. indicated that miR-214 expression is increased in the UUO model [54], in which XBP1 expression is downregulated in our study [17]. These findings indicate the possible mechanism involved in IRE1 α phosphorylation without XBP1 splicing. While, XBP1 deficiency or decreased nuclear expressions of XBP1 have been shown to contribute to pancreatic β cells dysfunction and keratinocytes senescence through activating IRE1 α [55, 56]. Depleting XBP1 induces the hyper-activation

of IRE1 α , leading to an impaired insulin secretion of β -cells [55]. Such a negative-feedback mechanism also participates in oncogenic H-Ras-induced premature senescence and subsequent tumor development [56]. Mechanisms through which the activated IRE1 α is involved in the pathogenesis of renal diseases remain unknown. Several plausible mechanisms have been suggested, including the cleavage of ER-localized mRNAs and microRNAs through regulating RIDD and through activating downstream effectors such as JNK. The link between JNK activation and renal injuries has been supported by findings that JNK co-opted with other signaling pathways to promote cell death, inflammation, and fibrosis [57].

Currently, the protective effect of XBP1 downregulation against I/R-induced kidney injury has been reported by Zhang et al. [58]. In the study, the renal function and pathological score significantly attenuated in XBP1 heterozygous mice subjected to I/R-induced AKI and a higher survival rate compared to the wild-type I/R group. Different from their approach, we used proximal tubular specific XBP1 conditional knockout mice to highlight the pathogenetic roles of XBP1 downregulation in renal epithelial, aggravating post-injured renal fibrosis. Furthermore, the profibrotic phenotypes of tubular cells were also observed in HK-2 with silenced XBP1, such as

cell cycle arrest and TGF β 1 secretion. Hence, our data support the concept that loss of XBP1 aggravates renal fibrosis.

XBP1s act as an adaptive UPR transcriptional regulator which participates in biological functions including helper T cell activation, myoblasts differentiation, and chondrocyte differentiation. Although researchers have identified potential targets of XBP1, the functional role of most of these XBP1 target genes remain poorly characterized. Our works demonstrated that Trap1 was one of the downstream targets of XBP1. Trap1 is one of the chaperons belonging to heat shock protein 90 family, which is located in mitochondrial and participates in maintaining mitochondrial function, proteostasis, and cell cycle progression [33]. Recent studies revealed that TRAP1 silencing results in cell cycle G2M phase progression in cancer cells [59–61]. In addition, overexpression of Trap1 can attenuate UUO-induced renal fibrosis and maintain mitochondrial integrity [35]; however, the underlying mechanism is still unclear. In our study, we revealed that the loss of XBP1 and Trap1 expression is consistent across different kidney injury models. On top of that, Trap1 is one of XBP1 downstream targets, which is able to relieve XBP1 silencing induced cell cycle arrest and decrease profibrotic factors production.

It has been considered that cell cycle arrest regulated by DDR is a protective mechanism to ensure that injured cells restore their functions [32]. However, prolonged cell cycle arrest caused by severe AKI may lead to maladaptive repair. Yang et al. showed that the transition of cell cycle S arrest to G2/M arrest had been observed in tubular cells of acute aristolochic acid nephropathy and various ischemic AKI models, reflecting a switch from an active repair response to a maladaptive repair [10]. Clearly, the increased probability of G2/M arrest may precipitate profibrotic factor production in damaged tubular epithelial cells. In our study, we demonstrated that the anti-fibrotic property of Trap1 was associated with its ability to limit genome instability. Growing evidence links XBP1 to the regulation of cell cycle and DNA repair [62–65]. For instance, deletion of XBP1 in yeast impeded DNA repair process [64], inhibited pseudohyphal growth on nitrogen-limited agar media due to the high expression of mitotic cyclin gene CBL2 [62]. Furthermore, XBP1 also has a role in IRE1 α -mediated upregulation of cyclin A, which in turn enhances cell proliferation in various prostate cancer cell lines [63]. Recently, Wang and Chao et al. showed that XBP1 silencing increased apoptosis and reduced cell proliferation in mouse granulosa cells. They found that the increase in cyclin E1 and the decrease in cyclin A1 and cyclin B1 contributed to S phase cell cycle arrest in XBP1-deficient cells [65]. These findings suggest that XBP1 plays

a central role in cell fate determination when cells face various stimuli in different cells.

Conclusions

The present study identified that the downregulation of XBP1 was profibrotic, and the process was mediated through autocrine and paracrine regulations in combination. The XBP1-Trap1 axis is an instrumental mechanism responsible for post-AKI fibrosis, which is a novel regulatory pathway.

Abbreviations

AKI: Acute kidney injury; APP: Amyloid precursor protein; ATF6: Activating transcription factor 6; Bip: Binding immunoglobulin protein; BUN: Blood urea nitrogen; CHOP: CAAT/enhancer-binding protein (C/EBP) homologous protein; CKD: Chronic kidney disease; CM: Conditioned medium; CTGF: Connective tissue growth factor; cKO: Conditional knockout; DDR: DNA damage response; eIF2 α : Eukaryotic translation initiation factor 2 α ; EMT: Epithelial-mesenchymal transition; ESRD: End-stage renal stage; ER: Endoplasmic reticulum; ERAD: ER associated protein degradation; EV: Empty vector; IBD: Inflammatory bowel disease; IRE1 α : Inositol-requiring enzyme 1 α ; JNK: C-Jun N-terminal kinase; LPS: Lipopolysaccharide; NTC: Negative control; Nx: Nephrectomy; PERK: PKR-like ER kinase; RIDD: Regulated Ire1 dependent decay; Scr: Serum creatinine; TGF β 1: Transforming growth factor β 1; Trap1: TNF receptor associate protein 1; UIRI: Unilateral ischemia–reperfusion injury; UNx: UIRI with contralateral Nx; UPR: Unfolded protein response; UUO: Unilateral ureteral obstruction; XBP1: X binding protein-1; XBP1s: Spliced isoform of XBP1; XBP1u: Unspliced isoform of XBP1.

Supplementary Information

The online version contains supplementary material available at <https://doi.org/10.1186/s12929-022-00828-9>.

Additional file 1: Table S1. Primer sequences of PCR, real-time PCR, and genotyping.

Additional file 2: Figure S1. UIRI causes prominent renal damage and development of fibrosis. (a) Diagram illustrates the timeline of the experiment. The left kidney of male C57BL/6 mice was subjected to renal ischemia/reperfusion injury (UIRI) and then sacrificed at different days as indicated. UDx: x days after UIRI. (b) PAS staining represents the accumulation of debris in the tubular lumen after UIRI. The arrowhead in the lower panel indicates debris. Scale bar indicates 200 μ m in 40x, 50 μ m in 200x. (c) qPCR assessment of the relative expression level of *Kim-1* mRNA. (d) Masson's trichrome staining shows the increased fibrosis fraction in kidney section after UIRI. Scale bar indicates 50 μ m in 200x. (e) Quantitative scores of interstitial fibrosis were assessed. (f and g) The expression of α -SMA was examined with western blot analysis and quantified. Data are expressed as means \pm SEM, n = 3–6 in each group. * P < 0.05 and *** P < 0.001, as compared with sham group. **Figure S2.** Loss of XBP1 expression is a universal characteristic in renal fibrosis models. (a) Western blot analysis showed the protein expression of α -SMA, XBP1u and XBP1s in UUO mice model. GAPDH was used as an internal control. (b–d) Quantification of relative protein expression levels of α -SMA, XBP1u and XBP1s. (e) Western blot analysis showed the protein expression of α -SMA, XBP1u and XBP1s in adenine diet mice model. GAPDH was used as an internal control. (f–h) Quantification of relative protein expression levels of α -SMA, XBP1u and XBP1s. N = 3–4 for each group, * P < 0.05, ** P < 0.01, and *** P < 0.001, as compared with sham or chow diet group. **Figure S3.** Proximal tubular conditional knockout mice blocked XBP1s activation. (a) Diagram illustrates SLC5a^{CreERT2}; XBP1^{fl/fl} mice. (b) After tamoxifen administration, mice were subjected to IP injection of 500 ng/g of Tunicamycin for 12 h. Western blot analysis showed protein expression of XBP1s after Tunicamycin induction in XBP1^{fl/fl} or XBP1^{cKO} mice. GAPDH was used as an internal control. (c) Immunofluorescence staining demonstrated XBP1 expression

in Tunicamycin treated mice kidneys. Scale bar: 250 μm . (d) XBP1s mRNA expression level was determined by semi-quantitative PCR. (e) qPCR assessment of the relative expression level of XBP1s mRNA. **Figure S4.** Proximal tubular XBP1 specific knockout mice were vulnerable to UIRI-induced kidney injury. (a) Diagram illustrates the experimental timeline of tamoxifen administration and UIRI with contralateral nephrectomy (Nx) surgery in XBP1^{fl/fl} and XBP1^{CKO} mice. (b and c) Blood urea nitrogen (BUN) and serum creatinine (Scr) levels were measured after 1 day of contralateral Nx. $N=3$ for each group. ** $P < 0.01$, and *** $P < 0.001$, as compared with XBP1^{fl/fl} Sham group. **Figure S5.** UIRI induces cell cycle arrest in G2/M phase. (a-d) The expression of chk1 and p21 in mice kidneys was evaluated with western blotting and quantified. GAPDH was used as an internal control. Data are expressed as means \pm SEM, $n=3-6$ in each group. * $P < 0.05$, ** $P < 0.01$, and *** $P < 0.001$, as compared with sham group. (e and f) Representative images of Ki67⁺ pHH3⁺ renal sections in (e) WT mice or (f) XBP1^{CKO} and XBP1^{fl/fl} mice subjected to UIRI or Sham operation. Selected areas indicated highly expressed double-positive tubules. Scale bar: 50 μm . (g) Number of Ki67⁺ pHH3⁺ tubular cells. Data are expressed as means \pm SEM. * $P < 0.05$, ** $P < 0.01$, and *** $P < 0.001$, as compared with XBP1^{fl/fl} sham group. ### $P < 0.001$ compared between indicated groups.

Additional file 3. Proteomic analysis of differentially expressed proteins in HK-2 cells silenced of XBP1 compared to scramble control.

Acknowledgements

We thank Dr. Laurie H. Glimcher for XBP1^{fl/fl} mice and the staff of the Second Core Laboratory, the Third Core Laboratory, and the Eighth Core Laboratory of the Department of Medical Research in the National Taiwan University Hospital for equipment and facility support.

Author contributions

JHC, CHW and JRJ conducted major experiments and data analysis. JRJ, JHC and CKC contributed to the design and the writing of the manuscript. CTC, JWH, KYH, and SHL provided reagents and critical comments. All authors read and approved the final manuscript.

Funding

This study was funded by Grants from the Taiwan Ministry of Science and Technology (MOST-104-2314-B-002-126-MY3, MOST-107-2314-B-002-027-MY3 and MOST 110-2314-B-002-130) and grants from the National Taiwan University Hospital (NTUH-106-S3574 and NTUH-107-S3826, NTUH.108-P02, NTUH-110-S5063).

Availability of data and materials

The datasets used and/or analyzed during the current study are available from the corresponding author on reasonable request.

Declarations

Ethics approval and consent to participate

All animal experiments were approved by National Taiwan University College of Medicine and College of Public Health Institutional Animal Care and Use Committee (IACUC No. 20150030, 20170540). Experimental protocols and animal care were provided according to the guideline for the care and use of animals established by National Taiwan University.

Consent for publication

Not applicable.

Competing interests

The authors declare that they have no competing interests.

Author details

¹Graduate Institute of Toxicology, College of Medicine, National Taiwan University, No.1 Jen Ai road section 1, Taipei 100, Taiwan. ²Department of Internal Medicine, College of Medicine, National Taiwan University, Taipei, Taiwan. ³Department of Integrated Diagnostics and Therapeutics, National Taiwan University Hospital, Taipei, Taiwan. ⁴Center for Biotechnology, National Taiwan University, Taipei, Taiwan.

Received: 22 February 2022 Accepted: 16 June 2022

Published online: 28 June 2022

References

- Mehta RL, Kellum JA, Shah SV, Molitoris BA, Ronco C, Warnock DG, Levin A. Acute Kidney Injury Network: report of an initiative to improve outcomes in acute kidney injury. *Crit Care*. 2007;11(2):R31.
- Wu VC, Wang CY, Shiao CC, Chang CH, Huang HY, Huang TM, Lai CF, Lin MC, Ko WJ, Wu KD, Yu CJ, Shu CC, Lee CH, Wang JY. National Taiwan University Study Group on Acute Renal F. and Taiwan Anti-Mycobacteria Investigation G. Increased risk of active tuberculosis following acute kidney injury: a nationwide, population-based study. *PLoS ONE*. 2013;8(7):e69556.
- Wu VC, Wu CH, Huang TM, Wang CY, Lai CF, Shiao CC, Chang CH, Lin SL, Chen YY, Chen YM, Chu TS, Chiang WC, Wu KD, Tsai PR, Chen L, Ko WJ. Long-term risk of coronary events after AKI. *J Am Soc Nephrol*. 2014;25(3):595–605.
- Saran R, Li Y, Robinson B, Abbott KC, Agodoa LY, Ayanian J, Bragg-Gresham J, Balkrishnan R, Chen JL, Cope E, Eggers PW, Gillen D, Gipson D, Hailpern SM, Hall YN, He K, Herman W, Heung M, Hirth RA, Hutton D, Jacobsen SJ, Kalantar-Zadeh K, Kovesdy CP, Lu Y, Molnar MZ, Morgenstern H, Nallamothu B, Nguyen DV, O'Hare AM, Plattner B, Pisoni R, Port FK, Rao P, Rhee CM, Sakhuja A, Schaubel DE, Selewski DT, Shahinian V, Sim JJ, Song P, Streja E, Kurella TM, Tentori F, White S, Woodside K, Hirth RA. US Renal Data System 2015 Annual Data Report: Epidemiology of Kidney Disease in the United States. *Am J Kidney Dis*. 2016;67(3 Suppl 1):S1–305.
- Wu VC, Wu PC, Wu CH, Huang TM, Chang CH, Tsai PR, Ko WJ, Chen L, Wang CY, Chu TS. The impact of acute kidney injury on the long-term risk of stroke. *J Am Heart Assoc*. 2014;3(4):e000933.
- Requiao-Moura LR, Durao Junior Mde S, Matos AC, Pacheco-Silva A. Ischemia and reperfusion injury in renal transplantation: hemodynamic and immunological paradigms. *Einstein (Sao Paulo)*. 2015;13(1):129–35.
- Basile DP, Anderson MD, Sutton TA. Pathophysiology of acute kidney injury. *Compr Physiol*. 2012;2(2):1303–53.
- Hsu RK, Hsu CY. The role of acute kidney injury in chronic kidney disease. *Semin Nephrol*. 2016;36(4):283–92.
- Grande MT, Sanchez-Laorden B, Lopez-Blau C, De Frutos CA, Boutet A, Arevalo M, Rowe RG, Weiss SJ, Lopez-Novoa JM, Nieto MA. Snail1-induced partial epithelial-to-mesenchymal transition drives renal fibrosis in mice and can be targeted to reverse established disease. *Nat Med*. 2015;21(9):989–97.
- Yang L, Besschetnova TY, Brooks CR, Shah JV, Bonventre JV. Epithelial cell cycle arrest in G2/M mediates kidney fibrosis after injury. *Nat Med*. 2010;16(5):535–43.
- Lovisa S, LeBleu VS, Tampe B, Sugimoto H, Vadhagara K, Carstens JL, Wu CC, Hagos Y, Burckhardt BC, Pentcheva-Hoang T, Nischal H, Allison JP, Zeisberg M, Kalluri R. Epithelial-to-mesenchymal transition induces cell cycle arrest and parenchymal damage in renal fibrosis. *Nat Med*. 2015;21(9):998–1009.
- Wu CF, Chiang WC, Lai CF, Chang FC, Chen YT, Chou YH, Wu TH, Linn GR, Ling H, Wu KD, Tsai TJ, Chen YM, Duffield JS, Lin SL. Transforming growth factor beta-1 stimulates profibrotic epithelial signaling to activate pericyte-myofibroblast transition in obstructive kidney fibrosis. *Am J Pathol*. 2013;182(1):118–31.
- Humphreys BD, Lin SL, Kobayashi A, Hudson TE, Nowlin BT, Bonventre JV, Valerius MT, McMahon AP, Duffield JS. Fate tracing reveals the pericyte and not epithelial origin of myofibroblasts in kidney fibrosis. *Am J Pathol*. 2010;176(1):85–97.
- Hetz C. The unfolded protein response: controlling cell fate decisions under ER stress and beyond. *Nat Rev Mol Cell Biol*. 2012;13:89.
- Fan Y, Xiao W, Lee K, Salem F, Wen J, He L, Zhang J, Fei Y, Cheng D, Bao H, Liu Y, Lin F, Jiang G, Guo Z, Wang N, He JC. Inhibition of reticulon-1a-mediated endoplasmic reticulum stress in early AKI attenuates renal fibrosis development. *J Am Soc Nephrol*. 2017;28(7):2007–21.
- Shu S, Zhu J, Liu Z, Tang C, Cai J, Dong Z. Endoplasmic reticulum stress is activated in post-ischemic kidneys to promote chronic kidney disease. *EBioMedicine*. 2018;37:269–80.

17. Chiang CK, Hsu SP, Wu CT, Huang JW, Cheng HT, Chang YW, Hung KY, Wu KD, Liu SH. Endoplasmic reticulum stress implicated in the development of renal fibrosis. *Mol Med*. 2011;17(11–12):1295–305.
18. Liu S-H, Yang C-C, Chan D-C, Wu C-T, Chen L-P, Huang J-W, Hung K-Y, Chiang C-K. Chemical chaperone 4-phenylbutyrate protects against the endoplasmic reticulum stress-mediated renal fibrosis in vivo and in vitro. *Oncotarget*. 2016;7(16):22116.
19. Harding HP, Zhang Y, Zeng H, Novoa I, Lu PD, Calton M, Sadri N, Yun C, Popko B, Paules R, Stojdl DF, Bell JC, Hettmann T, Leiden JM, Ron D. An integrated stress response regulates amino acid metabolism and resistance to oxidative stress. *Mol Cell*. 2003;11(3):619–33.
20. Ye J, Rawson RB, Komuro R, Chen X, Dave UP, Prywes R, Brown MS, Goldstein JL. ER stress induces cleavage of membrane-bound ATF6 by the same proteases that process SREBPs. *Mol Cell*. 2000;6(6):1355–64.
21. Lee K, Tirasophon W, Shen X, Michalak M, Prywes R, Okada T, Yoshida H, Mori K, Kaufman RJ. IRE1-mediated unconventional mRNA splicing and S2P-mediated ATF6 cleavage merge to regulate XBP1 in signaling the unfolded protein response. *Genes Dev*. 2002;16(4):452–66.
22. Park SM, Kang TI, So JS. Roles of XBP1s in transcriptional regulation of target genes. *Biomedicines*. 2021;9(7):791.
23. Hetz C, Chevet E, Oakes SA. Proteostasis control by the unfolded protein response. *Nat Cell Biol*. 2015;17(7):829–38.
24. Martin D, Li Y, Yang J, Wang G, Margariti A, Jiang Z, Yu H, Zampetaki A, Hu Y, Xu Q, Zeng L. Unspliced X-box-binding protein 1 (XBP1) protects endothelial cells from oxidative stress through interaction with histone deacetylase 3. *J Biol Chem*. 2014;289(44):30625–34.
25. Yoshida H, Oku M, Suzuki M, Mori K. pXBP1(U) encoded in XBP1 pre-mRNA negatively regulates unfolded protein response activator pXBP1(S) in mammalian ER stress response. *J Cell Biol*. 2006;172(4):565–75.
26. Yanagitani K, Imagawa Y, Iwakaki T, Hosoda A, Saito M, Kimata Y, Kohno K. Cotranslational targeting of XBP1 protein to the membrane promotes cytoplasmic splicing of its own mRNA. *Mol Cell*. 2009;34(2):191–200.
27. Kitamura M. Endoplasmic reticulum stress and unfolded protein response in renal pathophysiology: Janus faces. *Am J Physiol Renal Physiol*. 2008;295(2):F323–334.
28. Le Clef N, Verhulst A, D'Haese PC, Vervaeke BA. Unilateral renal ischemia-reperfusion as a robust model for acute to chronic kidney injury in mice. *PLoS ONE*. 2016;11(3):e0152153.
29. Jheng JR, Lau KS, Tang WF, Wu MS, Horng JT. Endoplasmic reticulum stress is induced and modulated by enterovirus 71. *Cell Microbiol*. 2010;12(6):796–813.
30. Chen JH, Chao CT, Huang JW, Hung KY, Liu SH, Tarng DC, Chiang CK. Early elimination of uremic toxin ameliorates AKI-to-CKD transition. *Clin Sci (Lond)*. 2021;135(23):2643–58.
31. Humphreys BD, Xu F, Sabbisetti V, Grgic I, Movahedi Naini S, Wang N, Chen G, Xiao S, Patel D, Henderson JM, Ichimura T, Mou S, Soeung S, McMahon AP, Kuchroo VK, Bonventre JV. Chronic epithelial kidney injury molecule-1 expression causes murine kidney fibrosis. *J Clin Invest*. 2013;123(9):4023–35.
32. Kishi S, Brooks CR, Taguchi K, Ichimura T, Mori Y, Akinfolarin A, Gupta N, Galichon P, Elias BC, Suzuki T, Wang Q, Gewin L, Morizane R, Bonventre JV. Proximal tubule ATR regulates DNA repair to prevent maladaptive renal injury responses. *J Clin Invest*. 2019;129(11):4797–816.
33. Joshi A, Dai L, Liu Y, Lee J, Ghahhari NM, Segala G, Beebe K, Jenkins LM, Lyons GC, Bernasconi L, Tsai FTF, Agard DA, Neckers L, Picard D. The mitochondrial HSP90 paralog TRAP1 forms an OXPHOS-regulated tetramer and is involved in mitochondrial metabolic homeostasis. *BMC Biol*. 2020;18(1):10.
34. Sisinni L, Maddalena F, Condelli V, Pannone G, Simeon V, Li Bergolis V, Lopes E, Piscazzi A, Matassa DS, Mazzoccoli C, Nozza F, Lettini G, Amoroso MR, Bufo P, Esposito F, Landriscina M. TRAP1 controls cell cycle G2-M transition through the regulation of CDK1 and MAD2 expression/ubiquitination. *J Pathol*. 2017;243(1):123–34.
35. Chen JF, Wu QS, Xie YX, Si BL, Yang PP, Wang WY, Hua Q, He Q. TRAP1 ameliorates renal tubulointerstitial fibrosis in mice with unilateral ureteral obstruction by protecting renal tubular epithelial cell mitochondria. *FASEB J*. 2017;31(10):4503–14.
36. Ishani A, Xue JL, Himmelfarb J, Eggers PW, Kimmel PL, Molitoris BA, Collins AJ. Acute kidney injury increases risk of ESRD among elderly. *J Am Soc Nephrol*. 2009;20(1):223–8.
37. Chevalier RL. The proximal tubule is the primary target of injury and progression of kidney disease: role of the glomerulotubular junction. *Am J Physiol Renal Physiol*. 2016;311(1):F145–161.
38. Cybulsky AV. Endoplasmic reticulum stress, the unfolded protein response and autophagy in kidney diseases. *Nat Rev Nephrol*. 2017;13(11):681–96.
39. Inagi R, Kumagai T, Nishi H, Kawakami T, Miyata T, Fujita T, Nangaku M. Preconditioning with endoplasmic reticulum stress ameliorates mesangio proliferative glomerulonephritis. *J Am Soc Nephrol*. 2008;19(5):915–22.
40. Zager RA, Johnson AC, Becker K. Acute unilateral ischemic renal injury induces progressive renal inflammation, lipid accumulation, histone modification, and “end-stage” kidney disease. *Am J Physiol Renal Physiol*. 2011;301(6):F1334–1345.
41. Arai S, Kitada K, Yamazaki T, Takai R, Zhang X, Tsugawa Y, Sugisawa R, Matsumoto A, Mori M, Yoshihara Y, Doi K, Maehara N, Kusunoki S, Takahata A, Noiri E, Suzuki Y, Yahagi N, Nishiyama A, Gunaratnam L, Takano T, Miyazaki T. Apoptosis inhibitor of macrophage protein enhances intraluminal debris clearance and ameliorates acute kidney injury in mice. *Nat Med*. 2016;22(2):183–93.
42. Madhusudhan T, Wang H, Dong W, Ghosh S, Bock F, Thangapandi VR, Ranjan S, Wolter J, Kohli S, Shahzad K, Heidel F, Krueger M, Schwenger V, Moeller MJ, Kalinski T, Reiser J, Chavakis T, Isermann B. Defective podocyte insulin signalling through p85-XBP1 promotes ATF6-dependent maladaptive ER-stress response in diabetic nephropathy. *Nat Commun*. 2015;6:6496.
43. Fedeles SV, So JS, Shrikhande A, Lee SH, Gallagher AR, Barkauskas CE, Somlo S, Lee AH. Sec63 and Xbp1 regulate IRE1α activity and polycystic disease severity. *J Clin Invest*. 2015;125(5):1955–67.
44. Ishikawa Y, Fedeles S, Marlier A, Zhang C, Gallagher AR, Lee AH, Somlo S. Spliced XBP1 rescues renal interstitial inflammation due to loss of Sec63 in collecting ducts. *J Am Soc Nephrol*. 2019;30(3):443–59.
45. Kaser A, Lee AH, Franke A, Glickman JN, Zeissig S, Tilg H, Nieuwenhuis EE, Higgins DE, Schreiber S, Glimcher LH, Blumberg RS. XBP1 links ER stress to intestinal inflammation and confers genetic risk for human inflammatory bowel disease. *Cell*. 2008;134(5):743–56.
46. Fang P, Xiang L, Huang S, Jin L, Zhou H, Zhuge L, Li J, Fan H, Zhou L, Pan C, Zheng Y. IRE1α-XBP1 signaling pathway regulates IL-6 expression and promotes progression of hepatocellular carcinoma. *Oncol Lett*. 2018;16(4):4729–36.
47. Chen C, Zhang X. IRE1α-XBP1 pathway promotes melanoma progression by regulating IL-6/STAT3 signaling. *J Transl Med*. 2017;15(1):42.
48. Zeng L, Zampetaki A, Margariti A, Pepe AE, Alam S, Martin D, Xiao Q, Wang W, Jin ZG, Cockerill G, Mori K, Li YS, Hu Y, Chien S, Xu Q. Sustained activation of XBP1 splicing leads to endothelial apoptosis and atherosclerosis development in response to disturbed flow. *Proc Natl Acad Sci U S A*. 2009;106(20):8326–31.
49. Grandjean JMD, Madhavan A, Cech L, Seguinot BO, Paxman RJ, Smith E, Scampavia L, Powers ET, Cooley CB, Plate L, Spicer TP, Kelly JW, Wiseman RL. Pharmacologic IRE1/XBP1s activation confers targeted ER proteostasis reprogramming. *Nat Chem Biol*. 2020;16(10):1052–61.
50. Madhavan A, Kok BP, Rius B, Grandjean JMD, Alabi A, Albert V, Sukiasyan A, Powers ET, Galmozzi A, Saez E, Wiseman RL. Pharmacologic IRE1/XBP1s activation promotes systemic adaptive remodeling in obesity. *Nat Commun*. 2022;13(1):608.
51. Dufey E, Bravo-San Pedro JM, Eggers C, González-Quiroz M, Urra H, Sagredo AI, Sepulveda D, Pihán P, Carreras-Sureda A, Hazari Y, Sagredo EA, Gutierrez D, Valls C, Papaioannou A, Acosta-Alvarez D, Campos G, Domingos PM, Pedoux R, Chevet E, Alvarez A, Godoy P, Walter P, Glavic A, Kroemer G, Hetz C. Genotoxic stress triggers the activation of IRE1α-dependent RNA decay to modulate the DNA damage response. *Nat Commun*. 2020;11(1):2401.
52. Duan Q, Chen C, Yang L, Li N, Gong W, Li S, Wang DW. MicroRNA regulation of unfolded protein response transcription factor XBP1 in the progression of cardiac hypertrophy and heart failure in vivo. *J Transl Med*. 2015;13:363.
53. Duan Q, Yang L, Gong W, Chaugai S, Wang F, Chen C, Wang P, Zou MH, Wang DW. MicroRNA-214 is upregulated in heart failure patients and suppresses XBP1-mediated endothelial cells angiogenesis. *J Cell Physiol*. 2015;230(8):1964–73.
54. Denby L, Ramdas V, Lu R, Conway BR, Grant JS, Dickinson B, Aurora AB, McClure JD, Kipgen D, Delles C, van Rooij E, Baker AH. MicroRNA-214

- antagonism protects against renal fibrosis. *J Am Soc Nephrol*. 2014;25(1):65–80.
55. Lee AH, Heidtman K, Hotamisligil GS, Glimcher LH. Dual and opposing roles of the unfolded protein response regulated by IRE1 alpha and XBP1 in proinsulin processing and insulin secretion. *Proc Natl Acad Sci U S A*. 2011;108(21):8885–90.
 56. Blazanin N, Son J, Craig-Lucas AB, John CL, Breech KJ, Podolsky MA, Glick AB. ER stress and distinct outputs of the IRE1alpha RNase control proliferation and senescence in response to oncogenic Ras. *Proc Natl Acad Sci U S A*. 2017;114(37):9900–5.
 57. Grynberg K, Ma FY, Nikolic-Paterson DJ. The JNK signaling pathway in renal fibrosis. *Front Physiol*. 2017;8:829.
 58. Zhang J, Zhang J, Ni H, Wang Y, Katwal G, Zhao Y, Sun K, Wang M, Li Q, Chen G, Miao Y, Gong N. Downregulation of XBP1 protects kidney against ischemia-reperfusion injury via suppressing HRD1-mediated NRF2 ubiquitylation. *Cell Death Discov*. 2021;7(1):44.
 59. Zhang X, Dong Y, Gao M, Hao M, Ren H, Guo L, Guo H. Knockdown of TRAP1 promotes cisplatin-induced apoptosis by promoting the ROS-dependent mitochondrial dysfunction in lung cancer cells. *Mol Cell Biochem*. 2020;476(2):1075–82.
 60. Palladino G, Notarangelo T, Pannone G, Piscazzi A, Lamacchia O, Sisinni L, Spagnoletti G, Toti P, Santoro A, Storto G, Bufo P, Cignarelli M, Esposito F, Landriscina M. TRAP1 regulates cell cycle and apoptosis in thyroid carcinoma cells. *Endocr Relat Cancer*. 2016;23(9):699–709.
 61. Condelli V, Piscazzi A, Sisinni L, Matassa DS, Maddalena F, Lettini G, Simeon V, Palladino G, Amoroso MR, Trino S, Esposito F, Landriscina M. TRAP1 is involved in BRAF regulation and downstream attenuation of ERK phosphorylation and cell-cycle progression: a novel target for BRAF-mutated colorectal tumors. *Cancer Res*. 2014;74(22):6693–704.
 62. Miled C, Mann C, Faye G. Xbp1-mediated repression of CLB gene expression contributes to the modifications of yeast cell morphology and cell cycle seen during nitrogen-limited growth. *Mol Cell Biol*. 2001;21(11):3714–24.
 63. Thorpe JA, Schwarze SR. IRE1alpha controls cyclin A1 expression and promotes cell proliferation through XBP-1. *Cell Stress Chaperones*. 2010;15(5):497–508.
 64. Tao R, Chen H, Gao C, Xue P, Yang F, Han JD, Zhou B, Chen YG. Xbp1-mediated histone H4 deacetylation contributes to DNA double-strand break repair in yeast. *Cell Res*. 2011;21(11):1619–33.
 65. Wang N, Zhao F, Lin P, Zhang G, Tang K, Wang A, Jin Y. Knockdown of XBP1 by RNAi in mouse granulosa cells promotes apoptosis, inhibits cell cycle, and decreases estradiol synthesis. *Int J Mol Sci*. 2017;18(6):1152.

Publisher's Note

Springer Nature remains neutral with regard to jurisdictional claims in published maps and institutional affiliations.

Ready to submit your research? Choose BMC and benefit from:

- fast, convenient online submission
- thorough peer review by experienced researchers in your field
- rapid publication on acceptance
- support for research data, including large and complex data types
- gold Open Access which fosters wider collaboration and increased citations
- maximum visibility for your research: over 100M website views per year

At BMC, research is always in progress.

Learn more biomedcentral.com/submissions

